ACTINIDE RESEARCH QUARTERLY

Ac Th Pa U Np Pu Am Cm Bk Cf Es Fm Md No Lr

Third Quarter 2019

PLUTONIUM FUTURES 2018 CONFERENCE ISSUE

NUMBER 2 OF 2

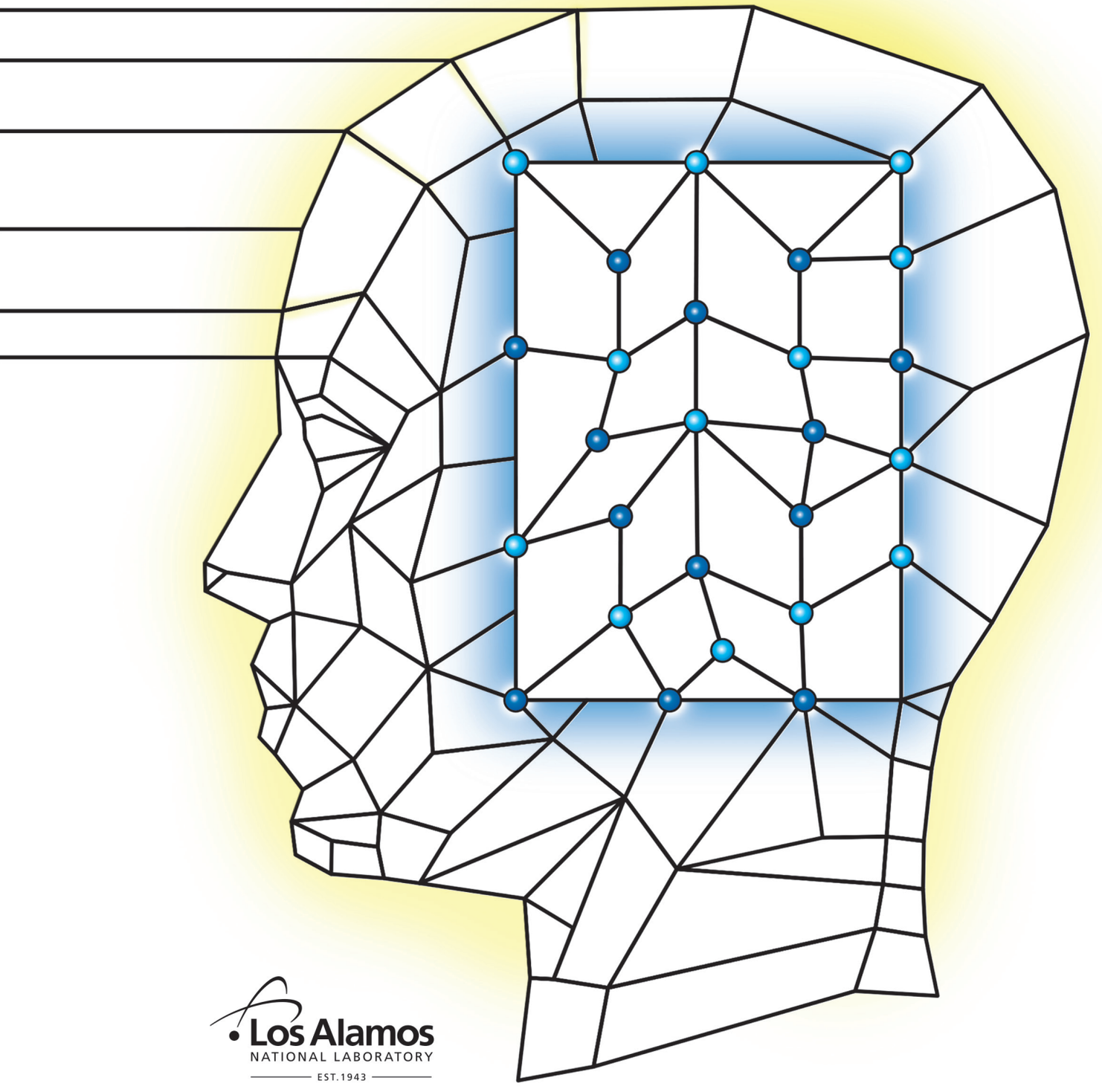

Los Alamos
NATIONAL LABORATORY
EST. 1943

Foreword

This is the second issue of the Los Alamos National Laboratory (LANL) Actinide Research Quarterly dedicated to honoring the Plutonium Futures—The Science 2018 conference held in San Diego, CA, and the scientists and engineers of the diverse scientific and technological disciplines that conduct plutonium and actinide research. This conference series provides a venue for the presentation and discussion of current topics on the physical, chemical, and engineering properties of plutonium and other actinide elements. We continue in this issue honoring the broad ranging topics presented at Plutonium Futures, including: environmental chemistry, metallurgy and materials science, surface science and corrosion, coordination chemistry, nuclear fuel-cycle, condensed matter physics, and detection and speciation analysis. The articles here represent some of the most exciting of research conducted by the global actinide research and technology community.

Dr. Terry C. Wallace, Jr., the eleventh Director of LANL and president of Los Alamos National Security, LLC, was the conference banquet speaker on Wednesday, September 12th. His presentation entitled "The Pu Unknown Unknowns" discussed the critical role Los Alamos has played in some of the most transformational discoveries of actinide science and technology during the 20th and 21st centuries. In particular, Wallace described the national laboratory's role in maintaining the nation's nuclear weapons stockpile and in protecting the nation through programs in nuclear counterproliferation and nonproliferation. As Director of LANL, Wallace described his stockpile stewardship responsibility of submitting the annual assessment of the Los Alamos weapons systems within the US nuclear stockpile to the President. In consideration of that role, he shared with the conference participants his concerns regarding uncertainties in aging processes of Pu and other materials components and the potential for impact to properties and performance of Los Alamos stockpile weapon systems. Wallace stated that his ability to conclude, with confidence, that the nation's strategic nuclear deterrent is reliable lies in Los Alamos' extensive expertise in modeling and simulation, physics, chemistry, and a whole host of other scientific and technological capabilities that provides the critical information which then feeds into the annual assessment.

The meeting concluded with the announcement of the next venue for the Plutonium Futures series. We look forward to another successful conference with enthusiasm and anticipation of new and exciting research on plutonium and the actinides. Here we mark the CEA Marcoule (commissariat à l'énergie atomique et aux énergies alternatives) proposal of hosting Plutonium Futures—The Science Conference 2020 planned for June 6–12, 2020 in Montpellier, France. This event will be a joint conference with CEA Marcoule Adalante 2020.

— Franz Freibert, Co-Chair Plutonium Futures 2018

About the cover: This image pairs with our previous issue, the first part in the Plutonium Futures 2018 conference series, which depicted the (pressure, temperature) phase diagram of elemental plutonium. The current issue cover represents how changes in these phases describe structural changes in the metallic crystal structure.

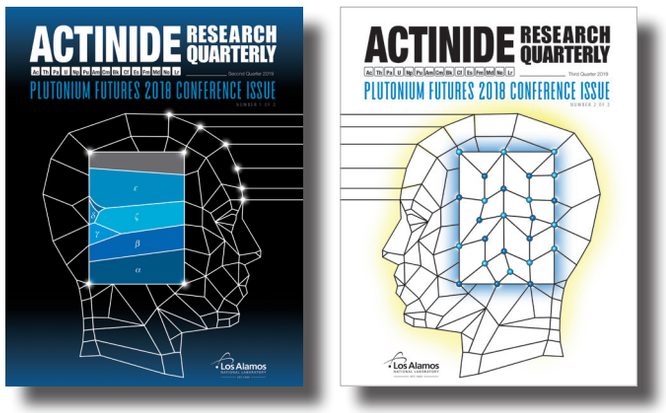

Contents

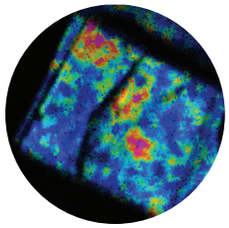

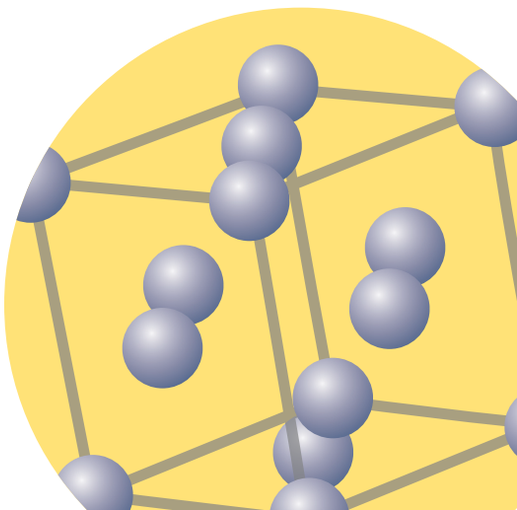

Brice Ravat

Brice Ravat, Scientist at CEA Valduc, France presented his invited talk titled "Metallurgy of PuGa Alloys: The Latest Insights into d-Phase Stability and Oxidation" *at Pu Futures 2018 as a plenary speaker in Plenary Session III.*

Metallurgy of PuGa Alloys: Insights into δ-Phase Stability and Oxidation

Brice Ravat, Benoît Oudot, Lionel Jolly, Fanny Lalire, Aurelien Perron, François Delaunay

CEA Valduc, F-21120 Is-sur-Tille, France

Plutonium displays highly unusual behavior that makes it the most complex element in the periodic table. Indeed, Pu metal has six allotropic phases between room temperature and its melting point (at ambient pressure). The stable phase at room temperature is the brittle α-phase (simple monoclinic). The most useful phase for metallurgical applications meanwhile is the δ-phase (face-centered cubic), stable from 315 to 457°C. It can be obtained at room temperature by alloying Pu with "δ-phase stabilizing" elements such as Al, Am, Ce, and Ga.

When the metastable δ-phase of PuGa alloy is cooled to sub-ambient temperatures, a partial transformation into the martensitic α'-phase occurs involving a large volume contraction of almost 20%. Martensitic transformation is a displacive and diffusionless phase-change process; thus, the product phase inherits the chemical composition of the parent phase. The crystal structure of the martensitic α'-phase is similar to that of the simple monoclinic α-phase with Ga atoms trapped in the lattice. The martensitic transformation kinetics of the PuGa alloys exhibit a time-temperature-transformation (TTT) diagram that takes the form of a "double-C" curve, the origin of which is still under debate (Fig. 1).

Heating PuGa alloys with high Ga content causes the reverse α'-to-δ transformation, which is direct and occurs through a burst martensitic mode that corresponds to a cascade of α' plates reverting to the δ-phase. With low Ga content, the reverse transformation has been found to be partially indirect before complete reversion to the δ-phase. However, the physics underpinning the behavior of Ga during this indirect reversion process is still unresolved.

As a further consideration, δ-Pu is very sensitive to corrosion, which can be severe in long-term storage under an inadequately controlled atmosphere. Although the corrosion of δ-Pu alloys has been studied for several decades, many questions remain about the nature and the arrangement of each phase forming the oxide scale (i.e., outer shell/surface layer), its individual growth, and the mechanisms governing the oxidation process.

In order to better understand the stability and reactivity of the important δ-phase, work has been performed over the last few years exclusively on a PuGa 1 at.% alloy (at the extreme limit of the δ metastability domain), studying the martensitic transformation at low temperature and under load, the entire reversion process, and oxidation of δ-Pu alloy with dry oxygen exposures at different temperatures.

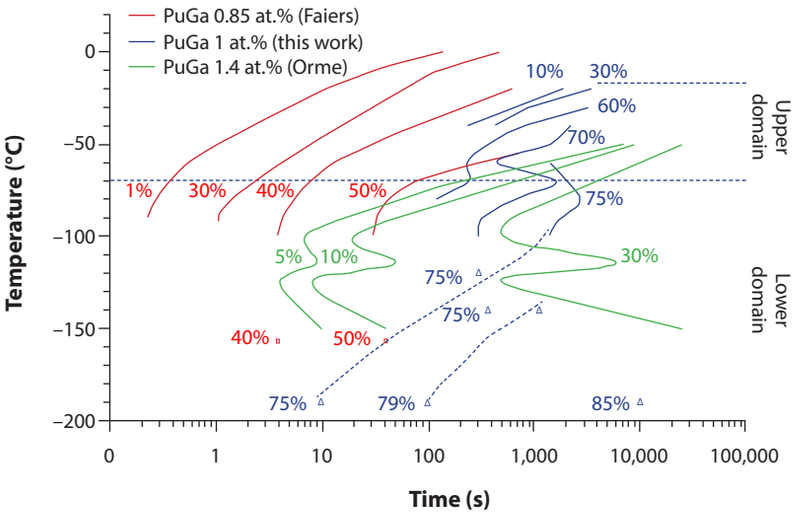

Figure 1. Time-temperature-transformation (TTT) diagram with percentages corresponding to the amount of martensitic transformation of PuGa alloys with 1, 0.85, and 1.4 at.% doping (blue—data from this work, red, and green, respectively). Triangles and squares are experimental results not taken into account in the fitting curves (solid curves). Two distinct domains can be identified from the double-C curve (indicated by dotted lines), whose origin is still under debate. We argue that this double-C curve for PuGa 1at.% alloy is related to two different accommodation modes leading to two different morphologies.

Martensitic transformation

The martensitic transformation kinetics were studied using in situ X-ray diffractometry (XRD) to investigate the effect of temperature. The kinetics exhibit an initial incubation period which may be related to the absence of favorable embryos which initiate the change. Solid-solid phase transformations are generally characterized by heterogeneous nucleation, with preferential nucleation sites such as inclusions, dislocations, grain boundaries, and vacancies. However, the nature of such sites in Pu alloys is still widely debated, and possible α and/or β precipitates/inclusions in the matrix might act as precursors for the martensitic transformation.

The incubation period is followed by a large acceleration of the transformation rate, which is associated with an autocatalytic nucleation process that controls the nucleation rate. This effect is taken into account in the Pati and Cohen kinetics formalism, which enables the incubation period and the large acceleration of the transformation kinetics to be reproduced, as observed in the isothermal kinetics at –20°C (Fig. 2).

The transformation rate subsequently decreases as it progresses and reaches saturation. The incomplete character of the transformation was not reproduced with a constant transformation energetic barrier ΔW. Using a variable ΔW factor was necessary to give an accurate description of the complete kinetics for all the transformation temperatures. The observed increase in ΔW suggests an accumulation of elastic/plastic strains in the δ-phase around the α'-phase that forms. These elastic stresses were confirmed by the observation of a cell parameter variation of the parent phase.

Martensite morphologies

The study has also shown that different martensite morphologies occur in the two domains of the TTT diagram. A feather-like morphology that may be attributed to elasto-plastic accommodation, as revealed by the sample surface macroscopic strain, occurs at relatively high temperatures (upper C-curve), whereas very thin parallel plates, reflective of elastic accommodation, appear at lower temperatures (lower domain), as shown in Fig. 3. Therefore, by impacting the dislocation motion the temperature of the isothermal hold influences the accommodation mechanisms.

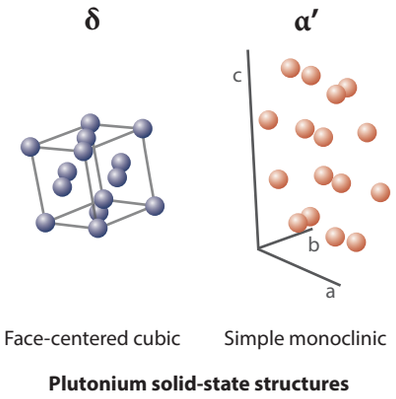

Plutonium solid-state structures

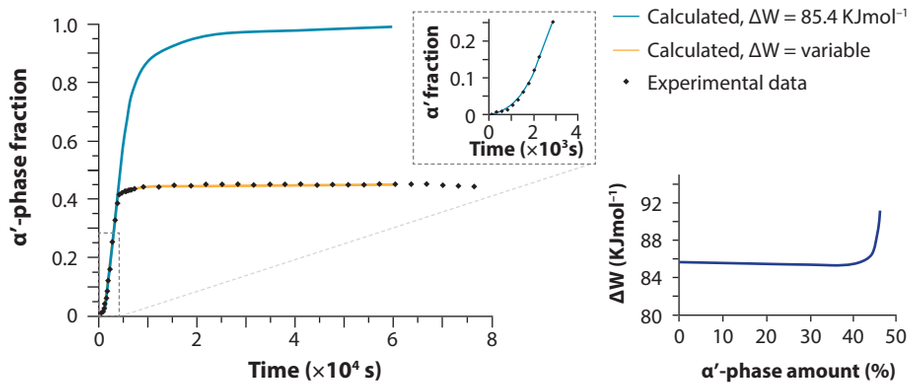

Figure 2. Theoretical and experimental kinetics for the martensitic transformation of the Pu phases δ → α' (*left*) keeping the temperature at –20°C. This shows that using a variable ΔW factor (orange line) is necessary for the computational model to match the experimental data (variability of ΔW is shown, *right*). Number of potential nucleation sites p = 9 × 10^{10} embryos cm^{-3} taken into account in the phenomenological approach to reproduce the kinetics data (notably the incubation time and the autocatalytic effect).

Martensitic transformation under applied stress

As discussed, modification of the stress state in the δ-phase strongly influences the martensitic transformation kinetics. Thus, an externally applied stress impacts the martensite transformation characteristics in the same way. Therefore we performed experimental and theoretical investigations of the martensitic transformation under elastic compressive and tensile stresses at low temperatures. These experiments required the design of original sample holders enabling stress to be applied at low temperature during both the in-situ XRD analysis and the dilatometry experiments.

It is necessary to determine the additional driving force associated with the applied stress to calculate the theoretical M_s temperature variations (during cooling, the M_s temperature is the point from which the martensitic transformation begins). This contribution of mechanical energy was assessed using the Patel and Cohen formalism, which considers the specific strain components related to the δ-to-α' phase transformation.

The additional driving force provided by the applied stress leads to a reasonably significant increase in M_s temperature, as revealed by the theoretical and experimental results which exhibit good agreement (Fig. 4). The linear increase in M_s temperatures versus applied stress matches the general mechanism of stress-assisted transformation, in which mechanical load provides a further driving force without changing the number of potential nucleation sites for an elastic load below the yield strength. The results also show that a compressive stress supports more energy than a tensile stress and contributes more significantly to the transformation.

Reversion process

Reversion of the martensite transformation upon heating is complex. Coupling experimental analyses (XRD and dilatometry measurements) with the CALPHAD (CALculation of PHAse Diagrams) method has made it possible to elucidate the mechanisms involved in the complete α'-phase reversion process.

The results showed that a portion of the α'-phase reverted directly into δ-phase after martensitic transformation, regardless of the sub-ambient quenching temperature (Eqn. 1), while the rest of the α'-phase reverted indirectly into the β

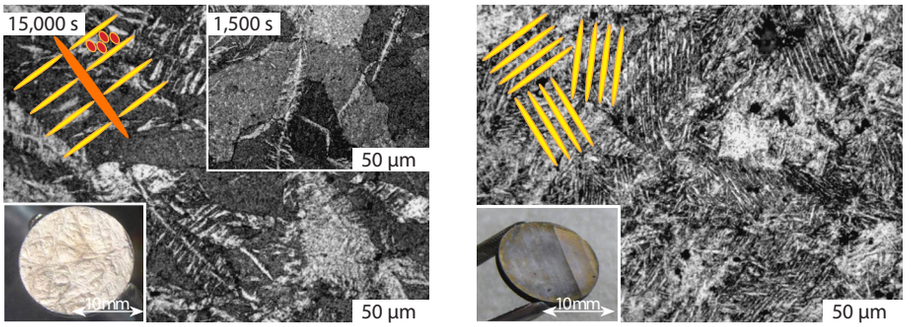

Figure 3. Optical micrographs showing the surface of PuGa 1 at.% sample transformed at (a) –20°C and (b) –196°C, and the different morphologies of the resultant α' phases. These images show that the temperature of the isothermal hold influences the accommodation mechanisms. The cartoon overlays are illustrations corresponding to the morphologies that can be observed in the optical micrographs. The yellow lines in (b) represent the thin parallel plate morphology observed at very low temperatures.

structure around 130°C. At this first stage of the reversion process, the concomitant observation of the drop in δ-phase lattice parameter and the great similarity between cell volumes of the incipient β structure and the pure Pu β-phase allowed us to conclude that the indirect martensite reversion involves the diffusion of Ga atoms, leading to gallium enrichment of the δ-phase ("δ_e") in addition to the emergence of areas of pure Pu (Eqn. 2).

(1) $\alpha'_{1at\%} \longrightarrow \delta_{1at\%}$

(2) $\alpha'_{1at\%} \longrightarrow \beta_{purePu} + \delta_e$

Between 130 and 200°C, no change in either the quantity of the β-phase or the Ga concentration in the enriched δ-phase was observed. Close to 210°C, allotropic transformation of the β-phase—which lies in the δ-phase matrix—into the pure Pu γ-phase occurred. Notably, a gradual temperature-dependent γ-to-δ reversion occurred alongside an increase in the cell parameter of the enriched δ-phase until it matched that of the PuGa δ-phase with an initial Ga content of 1 at.%. This highlights the Ga dilution process that occurred in the final step of the indirect reversion.

At the first reversion stage, where competition between the indirect and direct reversion modes occurs, thermodynamic calculations indicated that both modes are energetically possible, although the indirect reversion is effectively the most favorable. In fact, the Ga diffusion mechanism influences this competition. This has been experimentally demonstrated through dilatometry measurements performed at different heating rates, showing that the rate of direct reversion increases with heating rate. Indeed, a high heating rate limits the time for Ga diffusion, preventing the indirect reversion. Furthermore, the ratio between both reversion modes is affected by the initial α'-phase fraction, since the amount of indirect reversion is limited by the Ga solubility in the δ phase. Finally, high Ga concentration in the alloy promotes direct reversion. This is because its increase enhances the driving force of direct reversion at low temperature when indirect reversion is blocked due to the low diffusion of Ga.

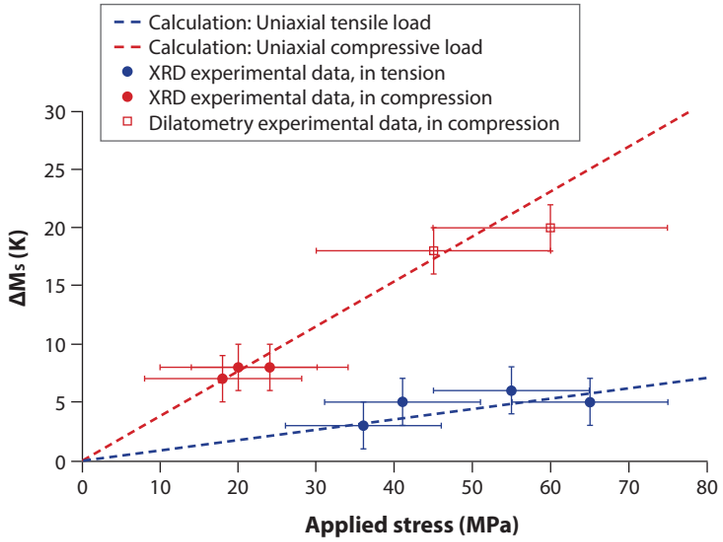

Figure 4. Theoretical (dashed lines) and experimental (solid dots) M_s temperature variations under applied tensile and compressive stresses using specific sample holders (M_s is the temperature from which the martensitic transformation begins). These data are in good agreement and show an increase in M_s temperature variations with increasing compressive and tensile applied stress.

Oxidation

The oxidation mechanism of δ-Pu under a dry oxygen atmosphere at different temperatures was studied using continuous in-situ XRD analysis (Fig. 5). The growth kinetics of each oxide present in the scale was characterized, including crystalline structure and thickness. An original Rietveld refinement method based on X-ray absorption versus scattering angle was developed to analyze the Pu oxide scale, which is assumed to consist of a layer stacking.

XRD analyses have confirmed the presence of PuO_2 and Pu_2O_3 during the oxidation process. The polymorphic character of Pu_2O_3 was also demonstrated with XRD data that reveal the cubic and hexagonal (α- and β-phases) crystallographic structures of the sesquioxide. In contrast, the observation of the body-centered monoclinic Pu structure, corresponding to the stable phase of pure Pu, was absolutely unexpected. Indeed, destabilization of the δ-phase resulting from oxidation has never been reported in the literature. It may be connected to the emergence of an area depleted in the δ-stabilizer element at the alloy-oxide interface. Nevertheless, the question about the location of the δ-stabilizing element remains basically open.

The oxidation kinetics can be clearly divided into two steps—initial parabolic-like behavior (as expected for a high-temperature oxidation process) followed by a linear growth stage. Analysis of the oxide layer thickening process reveals that the parabolic growth stage results mainly from the thickening of the α-Pu_2O_3 layer. During this stage the outer PuO_2 and inner β-Pu_2O_3 layers remain thin and stable in comparison with the intermediate α-Pu_2O_3 layer, which thickens continuously.

During the linear growth stage PuO_2 contributes to the accelerated oxidation. The enhanced PuO_2 growth can be explained by the presence of cracks and spalls at the sample surface, as revealed by scanning electron microscopy (SEM) analyses. The cracking of the oxide scale acts as a diffusion "short-circuit" allowing a large inflow of oxygen into the oxide scale, leading to a porous scale essentially composed of PuO_2. The appearance of cracks is assumed to stem from the development and accumulation of compressive stresses inside the oxide scale and particularly in the α-Pu_2O_3 layer (the predominant oxide formed during the parabolic growth stage). Thus, when the stress exceeds the cohesive forces, stress relaxation may occur by local buckling, cracking, or detachment of the oxide scale. Due to the fragility of the oxide scale, this causes the emergence of the observed cracks at the surface of the oxide scale.

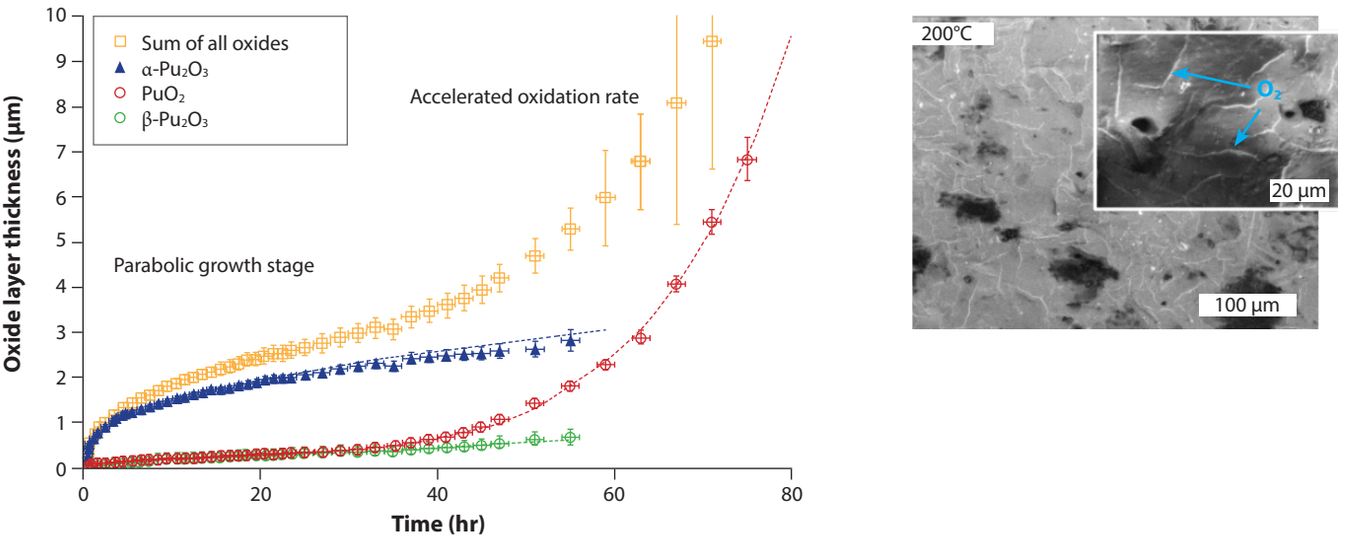

Figure 5. Thickness of overall oxide layer, PuO_2, α- and β-Pu_2O_3 scales deduced from XRD analysis during isothermal exposure at 200°C under a dry atmosphere of 100 mbar of O_2. The overall growth rate is driven by the increase in different oxides at different stages—the initial parabolic growth is dominated by the middle layer of α-Pu_2O_3 (blue), whereas the subsequent linear growth period is driven by an increase in outer layer PuO_2 (red), induced by surface cracking acting as a "short circuit" for oxygen diffusion (SEM picture of oxide scale, *right*).

Summary

We have obtained new insights into several aspects of the martensitic transformation in Pu-Ga alloys, including transformation mechanisms, kinetics, and martensite (Pu alloy) morphologies versus temperature and applied stress. The results demonstrated different martensite morphologies related to different accommodation mechanisms, and an autocatalytic character for the isothermal martensitic nucleation process, in addition to a large sensitivity to elastic and plastic strain. This reflects a high sensitivity of the energy barrier for nucleation to the α' phase; however, it is also responsible for the incomplete nature of the transformation. Hence, one major conclusion was that internal stresses play an important role.

The impact of external stresses was investigated. M_s temperatures for compressive and tensile loads were predicted by calculating the driving force (mechanical work) using the Patel and Cohen model, which showed good agreement with experimental results. The entire martensite reversion process was studied, showing heating involves two competing modes, namely direct and indirect reversion; the latter is associated with a Ga diffusion process that governs the ratio between these reversion modes. More precisely, our study demonstrates that this indirect reversion process occurs with Ga-enrichment of the remaining δ-phase and emergence of pure Pu β- and γ-phases before the complete recovery of the δ-phase.

Oxidation of δ-Pu alloy was examined using dry O_2 at different temperatures which destabilized the δ-phase and created a pure Pu β-phase. The oxide growth kinetics began with a parabolic stage, resulting mainly from the growth of an α-Pu_2O_3 layer in which a compressive stress state seems to develop as it thickens, leading to surface cracking. This acts as a "short circuit" for oxygen diffusion and is responsible for the linear growth of a porous oxide scale consisting essentially of PuO_2.

Although new findings over the last decade have improved our knowledge about plutonium alloys, many questions remain unanswered. Hence, plutonium metallurgy remains an exciting field for future exploration.

Further reading:

1. *F. Lalire, B. Ravat, B. Oudot, B. Appolaire, A. Perron, E. Aeby-Gautier, F. Delaunay, Acta Mater. 2017, 123, 125.*
2. *B. Ravat, B. Oudot, A. Perron, F. Lalire, F. Delaunay, J. Alloys and Comp. 2013, 580, 298.*
3. *A. Perron, B. Ravat, B. Oudot, F. Lalire, K. Mouturat, F. Delaunay, Acta Mater. 2013, 61, 7109.*
4. *B. Ravat, L. Jolly, B. Oudot, A. Fabas, H. Guerault, I. Popa, F. Delaunay, Corros. Sci. 2018, 138, 66.*
5. *B. Ravat, F. Lalire, B. Oudot, B. Appolaire, E. Aeby-Gautier, J. Pansiot, F. Delaunay, Materialia 2019, 6, 100304.*

Paul Tobash

Paul Tobash is a Scientist at Los Alamos National Laboratory, New Mexico. He presented his talk titled "Progress on the thermophysical properties of some plutonium alloys and compounds" *at Pu Futures 2018 in the Metallurgy and Materials Science II technical session.*

Leading Insight into the Complexities of Plutonium

Paul H. Tobash
Los Alamos National Laboratory, Los Alamos, New Mexico 87545

Actinide science offers many challenges at the intersection of chemistry, materials science, condensed matter physics, and metallurgy. Specifically, plutonium (Pu) resides precisely at this crossing where one has the ability to study a wealth of unique questions related to phase stability, thermophysical properties, surface/corrosion effects, aging, mechanical behavior, and structural motifs. Many of these areas include longstanding questions such as the true electronic ground state and nature of plutonium's 5f electrons (that cannot be treated as completely localized or delocalized), the establishment of a deformation-mechanism map for comprehending mechanical behavior in α- and δ-Pu, and the complex structural transitions and associated changes in atomic volume when α-Pu is heated and progresses through six distinct crystallographic phases. This sophisticated element offers a playground of exciting research areas which appeal to a multitude of scientific backgrounds.

Another exciting aspect to Pu science is that these questions can be approached from a number of avenues which frequently relate to each other, although this can often generate more questions. This is not a roadblock but instead helps establish new working hypotheses. Many of these results are included in the forthcoming and long-awaited update of the Plutonium Handbook—a significant achievement that discusses the latest in Pu science and the work of a multitude of actinide science experts (see p20). It is important that the momentum in Pu science is maintained and this work engages new and talented scientists. This not only includes fellow colleagues at Los Alamos National Laboratory (LANL) but also our domestic national laboratories, university collaborators, and the international community. The Pu Futures conference delivers an ideal setting for this dialog, as it is perfectly sized and appropriately focused on research in order to address the three main goals effectively outlined in the Integrated Pu Science and Research Strategy. I personally believe that we are witnessing a renaissance in Pu science, and the next few years will offer exciting results from our research on Pu-containing materials, laboratory infrastructure, and workforce of actinide scientists in whatever metric one chooses as an assessment.

Plutonium metallurgy offers a rich landscape of materials to study both from its variety of microstructures to its thermophysical properties and strong electronic correlations. This regime can span the compositional Pu alloys, eutectic phases, and ordered intermetallic compounds. A recent chapter in the revised Plutonium Handbook provides a detailed account of the structure and properties associated with Pu binary and ternary intermetallic compounds in addition to a review discussing preparation and measurement of these materials. Intriguing behavior in Pu intermetallics is exemplified by the emergence of properties such as long-range ordered magnetism in $PuIn_3$ and instances of unconventional superconductivity in $PuCoGa_5$, $PuCoIn_5$, and $PuRhIn_5$ (T_c = 18.5, 2.5, and 1.1 K respectively). This three-part summary is devoted to recent results from the systematic characterization of Pu alloys and compounds. These materials include Pu alloys with low weight-percent Ga (Pu with 0.18 and 0.63 wt.% Ga, which is 0.614 and 1.425 at.% Ga, respectively) and high weight-percent Ga δ-Pu alloys, in addition to plutonium monocarbide (PuC_{1-x}) and iron (Pu_6Fe) phases.

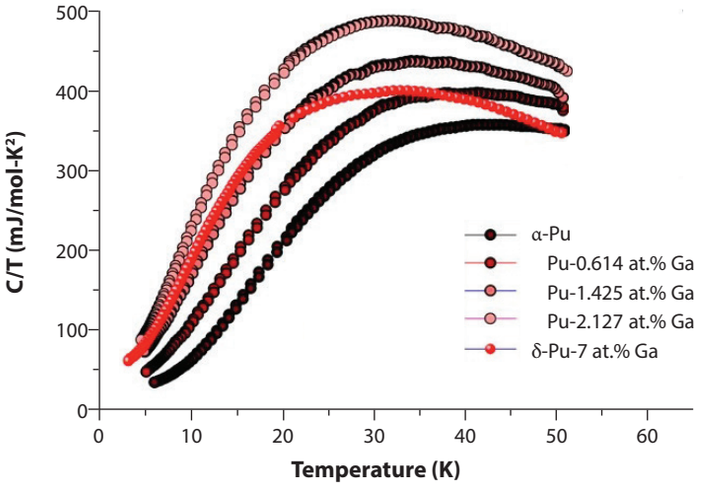

Figure 1. Compiled specific heat data for Pu materials in this study plotted as T (K) versus C/T (mJ/mol-K^2). This data reflects differences in the metallic phase measured at low temperatures. Note the general trend of the low temperature heat capacity curves with the exception being the Pu-7 at.% Ga stabilized sample (primary red) which did not show the α'-Pu phase forming upon cooling.

Section 1: Low-temperature heat capacity studies of Pu alloys

Performing thermophysical property measurements on actinide materials is important for characterization and probing electronic structure. This is especially true for elemental Pu and Pu-containing materials where many questions still remain regarding low-temperature physics. Over the past decade there have been numerous examples of intriguing physical behavior in many flux-grown crystals and alloys, including unconventional superconductivity, complex magnetism, paramagnetism, and additionally, how these properties are affected by radiation damage or aging. Measurements were obtained for magnetic susceptibility, heat capacity, and electrical resistivity, in addition to other properties for all of these cases. These have allowed more detailed studies of the Pu 5f electrons' dual nature in a variety of crystal structures and coordination environments (5f electrons exhibit intermediate behavior between completely itinerant and localized regimes). Plutonium's alpha particle radioactivity creates an additional safety challenge for data collection; it is therefore important that the experimentalist can obtain high-quality data while keeping the measurement system and sample holder free of radioactive contamination that may spread during measurements.

Specific heat measurements were performed using a commercially-available physical property measurement system (PPMS) from Quantum Design. Samples typically weighed around a few milligrams and were fixed onto the platform of a heat capacity puck using Apiezon N-grease. An initial measurement (an addenda measurement) of the heat capacity puck and the grease was performed without the sample. The sample was then measured and the contribution was subtracted from the addenda data. For the radioactive sample measurement, a brass cap was placed on the top of the sample puck and a small G10 plug was carefully fitted into the bottom hole opening of the puck to ensure that the sample was fully contained inside the sample holder and prevent the rare chance that it would fall off the sapphire platform into the sample chamber. Once the holder was assembled, it was carefully surveyed for radioactive contamination before being moved into the measurement system.

The measured alloys were homogenized at 450°C for 250 hours before being used for the heat capacity measurements. The as-cast microstructure of the Pu-0.614 at.% Ga sample contained both Ga-rich cores and Ga-depleted regions, but after homogenization, regions of combined α-/δ-Pu in addition to pure α-Pu regions were observed. The Pu-1.425 at.% Ga sample had an as-cast microstructure consisting of Ga-rich cores and regions that resembled α-Pu, while the homogenized sample developed a δ-Pu grain structure without any coring and grain sizes on the order of 50-55 microns.

Table 1. Sommerfeld coefficients for measured heat capacity materials.

Pu sample	Sommerfield coefficient (mJ/mol-K^2)
α-Pu	20(2)
Pu-0.614 at.% Ga	28(2)
Pu-1.425 at.% Ga	41(2)
Pu-2.127 at.% Ga	48(2)
δ-Pu-7 at.% Ga	48(2)

Heat capacity studies also included measurements on α-Pu, δ-Pu-2 at.% Ga, and δ-Pu-7 at.% Ga in order to observe the evolution of the low-temperature data. Samples weighed approximately 1–1.5 mg in order to overcome the self-heating effects of the material caused by self-irradiation; they were all cooled to a base temperature (~5K) over a 16 hour period. As can be seen from the data in Fig. 1, all of the samples, with the exception of δ-Pu-7 at.% Ga, demonstrate similar low-temperature behavior with transformation to the α'-Pu structure at these temperatures (α'-Pu represents the α structure of Pu with trapped dopants such as Ga). This transformation would not be expected in the δ-Pu-7 at.% Ga sample as shown by the red heat capacity curve.

The low-temperature regime was analyzed by plotting the data as T^2 (K^2) versus C/T (mJ/mol-K^2) in order to extract a Sommerfeld coefficient for each composition (results summarized in Table 1). The transformation of the δ-Pu alloys to α'-Pu can also be observed using electrical resistivity measurements. It is important to note that depending on the rate of cooling, the onset of this transition can be changed—this will be the focus of a future study. More recently, the results of these heat capacity measurements in conjunction with excitation levels and entropy contributions were utilized for a 2019 Nature Communications publication entitled "Phase stabilization by electronic entropy in plutonium" in which first time magnetostriction measurements on Pu were performed and shed light on better understanding the modeling of the 5f electrons of Pu.

Section 2: Characterization of binary PuC

Plutonium carbides have been extensively studied for their possible application as fuel elements in fast breeder reactors. The advantages of these materials stem from their high-power densities and larger thermal conductivities compared to oxides.

The "as-cast" PuC sample was analyzed by scanning electron microscopy (SEM) using an FEI Quanta instrument. The inner surface of the arc-melted button was probed, which was exposed to an ambient air environment for approximately one year after synthesis at Florida State University (FSU). The sample was mounted onto the aluminum SEM sample stub using copper tape and analyzed in its current form without any surface preparation or polishing; the sample had a shiny luster on the surface being characterized.

The PuC sample was arc-melted and subsequently annealed. The compound crystallizes with an NaCl structure type (Fig. 2). Plutonium monocarbide is better represented as a sub-stoichiometric compound, PuC_{1-x}; X-ray analysis showed a value of 42.5 at.% carbon.

Figure 2, *right*. Unit cell of cubic PuC, which shows an NaCl type structure; Pu = purple, C = red. X-ray diffraction analysis gave unit cell parameters of 4.9518(2) Å and a density of 14.00 g/cm^3.

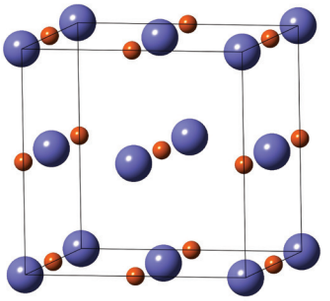

Figure 3, *below*. Scanning electron microscopy (SEM) images for the arc-melted PuC surface: (a) Porous morphology, major phase (8800x magnification); (b) Dendritic morphology, minor phase (11000x magnification).

(a) Porous morphology

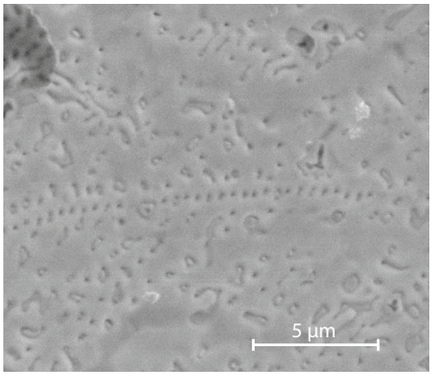

(a) Dendritic morphology

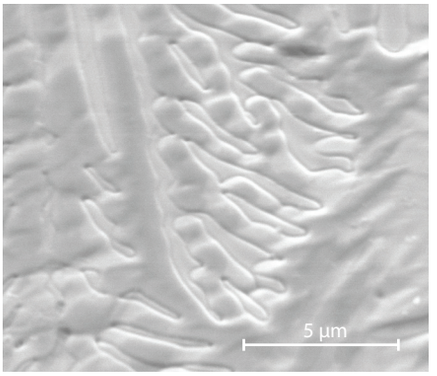

The samples were examined using SEM (Fig. 3). The majority of locations probed showed a porous-like structure while a small portion of the samples displayed dendritic or a feather-like morphology—Fig. 3a shows one of these surface structures with numerous pores present on the exterior along with some grain boundaries. Fig. 3b meanwhile shows another type of surface that can be described as lamellar and dendritic fingers of PuC material. These morphologies are consistent with those reported by Rosen and co-authors in a 1963 article published in the Journal of Nuclear Materials entitled "Metallographic and X-ray observations of Pu-C alloys".

At the uppermost point of the arc-melted button, a well-defined grain structure was found which provided an estimate of the general grain size present on the surface of the "as-cast" piece. The grains located at that region were well under 10 microns in diameter. Overall, the surface was very clean and only a small amount of oxide was present even after a long time sitting in an unprotected atmosphere (approximately one year).

The heat capacity of the PuC sample was measured after one year aging and also after annealing at an elevated temperature of 600°C for four days (Fig. 4). There was a distinct change in the specific heat curves in which long-range antiferromagnetic order appeared at approximately 98 K (Néel temperature). Additionally, the effect on the electronic correlations in the system was observed from the fact that the Sommerfeld coefficient showed a significant change in value between the aged and annealed samples (77.5 and 52.4 mJ/mol-K^2 respectively).

Section 3: Preliminary studies on Pu_6Fe

When Fe is present in Pu metal at concentrations above approximately 200 ppm, a eutectic compound (Pu_6Fe) forms when it is cooled below approximately 412°C. Chemical separations or refinement techniques of metals can often introduce

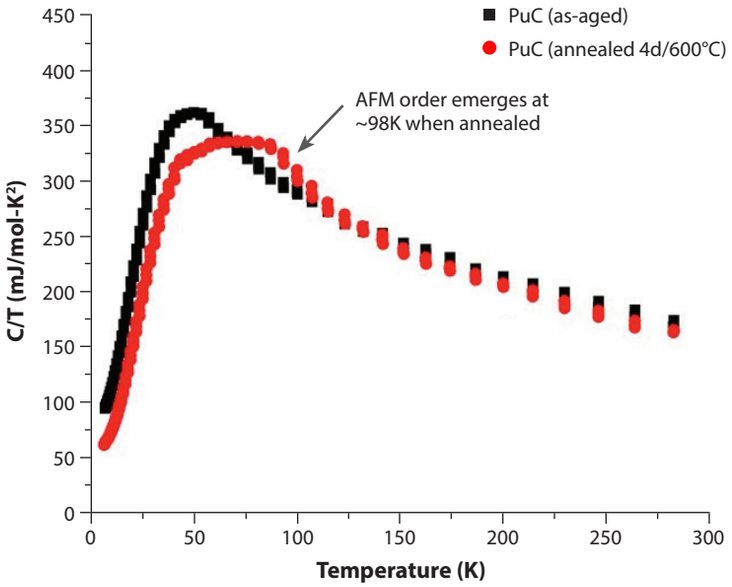

Figure 4. Specific heat data for the as-aged and annealed PuC sample, showing a significant change after the annealing process. γ (as-aged) = 77.5 mJ/mol-K², γ (annealed) = 52.4 mJ/mol-K². Data is plotted as T (K) versus C/T (mJ/mol-K²).

unintentional impurities into the final product. These impurities, even in small concentrations, can initiate a number of effects such as the introduction of precipitates into the crystal lattice, heterogeneity, or unwanted by-product formation, all of which affect the alloy's grain structure. A likely source for Fe impurities in Pu metal may derive from the well-known PUREX process, described by the reduction process in Eqn. 1 below (see the article by Hixon on p22 for more information on Pu redox chemistry).

$$(1) \qquad Pu^{4+} + Fe^{2+} \xrightarrow{NH_2SO_3^-} Pu^{3+} + Fe^{3+}$$

In the process of developing a metal-hydride-precursor method for making Pu_6Fe, we recently discovered a novel deuteride with the proposed formula Pu_6FeD_x ($15 < x < 17$). The presence of second-phase compounds, even at low concentrations, can influence many important properties of Pu alloys, including phase stability, microstructure and its evolution, and thermophysical properties. We reasoned that in order to consider the effects of Pu_6Fe in Pu alloys, we must start with developing a sound understanding of the intermetallic and its hydride in isolation.

Deuterium has a dramatic effect on the microstructure of the δ-Pu 2 at.% Ga sample (Fig. 5). The difference is observed from the transformation of Pu_6Fe wetting the grain boundaries of the δ-Pu grains to the spheroidization of ternary Pu_6FeD_x precipitates. The purpose of this study was to more closely examine not only the separate binary and ternary compounds but also their effects on the microstructure and properties of δ-Pu alloys.

The Pu_6Fe crystal structure (Fig. 6) is isostructural with U_6Fe, therefore it is likely that the deuteride (Pu_6FeD_x) shares the same structure with the reported compound U_6FeH_{15}. The two structures of Pu_6Fe and the ternary deuteride are closely related and both are composed of distorted octahedral units forming open cavities that are important for accommodating the deuterium atoms. Upon deuteration, the structure undergoes a transformation from tetragonal to cubic symmetry, similar to the β-UH_3 structure as provided from the $U_6Fe + 7.5\ H_2 \rightarrow U_6FeH_{15}$ reaction. We propose that the mechanism of the Pu_6Fe/D_2 reaction is most likely identical to U_6Fe/H_2; this will be the focus of a future study.

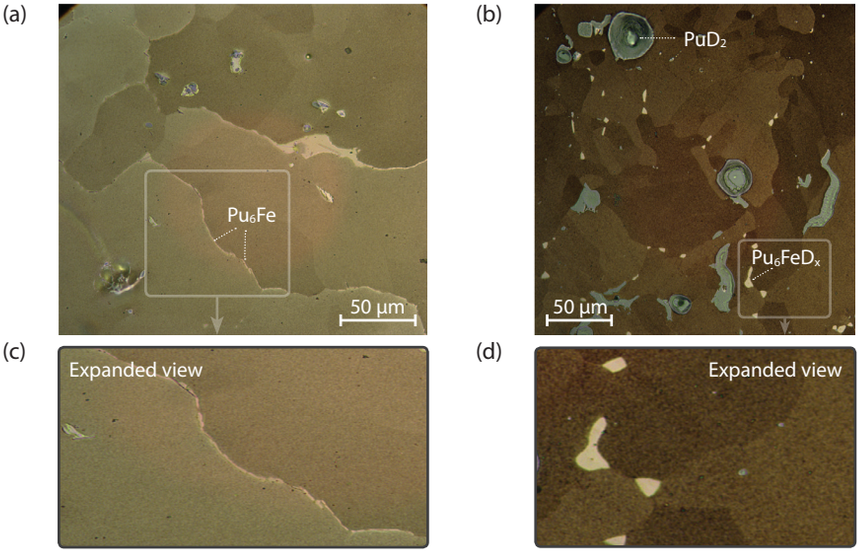

Figure 5. Microstructures (500×500 µm) of (a) an Fe-containing δ-Pu sample that shows Pu_6Fe wetting the δ-Pu grain boundaries, and (b) the same Fe-containing δ-Pu sample when the reaction of dissolved deuterium results in the formation of Pu_6FeD_x (white precipitates); the grey spots are excess PuD_2. Expanded areas of (c) Pu_6Fe wetting at δ-Pu grains and (d) Pu_6FeD_x precipitates.

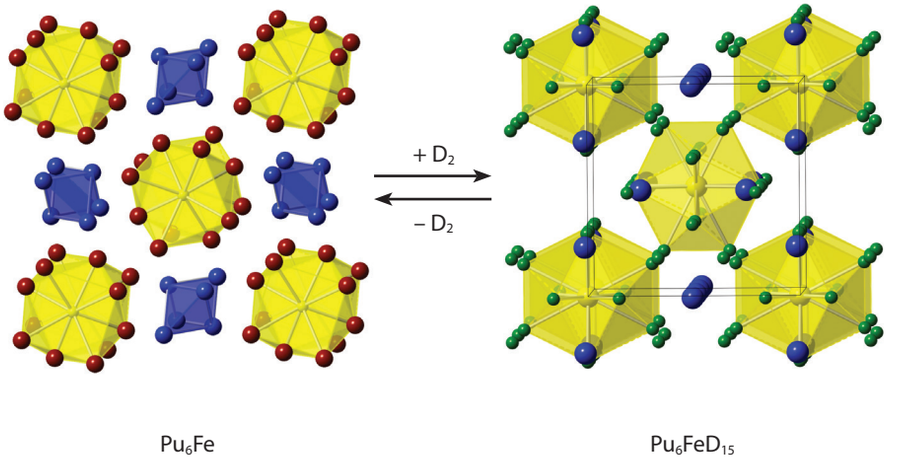

Figure 6. The crystal structures of Pu_6Fe and Pu_6FeD_{15} showing the proposed molecular-level change of a tetragonal to cubic lattice. This transformation will be specifically examined with theoretical calculations.

The sample displayed minimal unalloyed character with small peaks at the $\alpha \rightarrow \beta$, $\beta \rightarrow \gamma$, and $\gamma \rightarrow \delta$ Pu phase transitions. Analysis of relative heats for the given sample size indicates the sample analyzed with differential scanning calorimetry (DSC) was approximately 90% Pu_6Fe, a fairly good yield for this method and the best attempt so far for a bulk Pu_6Fe sample (Fig. 7).

During the reaction of Pu_6Fe from blended Fe and PuD_2 powder at 420°C it was noted that the equilibrium deuterium pressure was far too low for PuD_2 at that temperature. The temperature was varied and equilibrium D_2 pressures were obtained to produce the free energy plot shown in Fig. 8. The data show that the free energy of formation favors deuterium precipitation in the Fe compound over PuD_2.

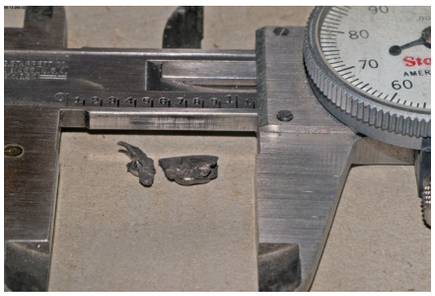

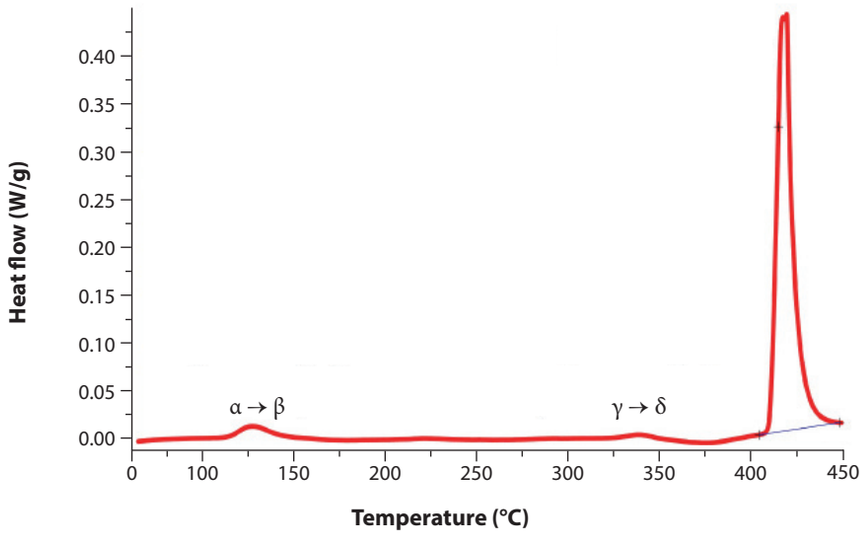

Figure 7. *Above*: The bulk sample of Pu_6Fe (~1.5g) synthesized in the Sievert's apparatus. *Right*: The melting point scan using differential scanning calorimetry, showing a melt peak (large peak) at the expected temperature of 412°C.

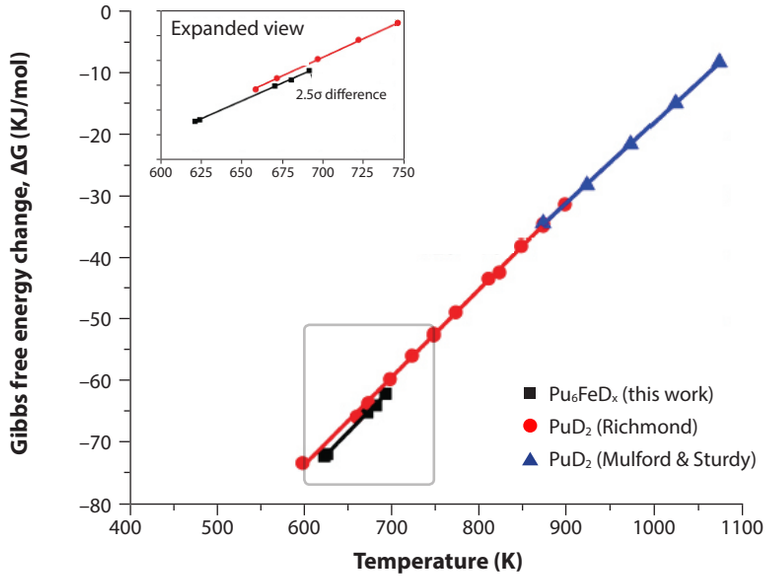

Figure 8. Thermodynamic evidence for the formation of Pu_6FeD_x during the synthesis of Pu_6Fe. The entropy difference observed between PuD_2 and Pu_6FeD_x (expanded area) was repeated and confirmed several times.

Summary: My personal vision for the direction of Pu science at LANL

The results described above were performed over the last few years and supported a variety of science programs at LANL. As discussed, understanding basic thermophysical properties of elemental Pu and its compounds from a fundamental perspective is important especially given the complexity of Pu. Heat capacity studies show the evolution of the electronic correlations present in these materials at low temperature as a function of the Ga concentration along the series (Section 1). The application of these results to the recent 2019 publication in Nature Communications will attempt to build upon our understanding of plutonium's 5f electrons and the most accurate way to model them in our theoretical calculations. The characterization of the PuC sample showed that its microstructure contained some very interesting features as evidenced from SEM (Section 2). Preliminary heat capacity data from after the sample was aged gave a noticeable change in its magnetic ordering and a different Sommerfeld coefficient. Finally, studies on the unique eutectic compound Pu_6Fe showed how this intermetallic compound affects the microstructure of δ-Pu and a ternary compound that forms under deuteration of this matrix (Section 3).

Maintaining this momentum in new material discovery and fundamental structure/property studies is important and will be most effective through the continuation of our strong Pu science capabilities, growth and enhancement of our laboratory spaces, attraction and retention of actinide scientists, and finally meetings such as the Pu Futures conference that allow for scientific collaboration in all aspects of Pu science. It is also essential to compile all of the above stated information in compendiums such as the recently revised Pu Handbook (see p20). This serves as an important reference for the next generation of actinide scientist to utilize and make the most of in their scientific careers. At the forefront of our experimental infrastructure and capabilities is the construction of a new Pu materials research laboratory space at LANL. This new building, the Radiological Laboratory Utility Office Building (RLUOB), was made possible following the decommissioning of the 65-year-old Chemistry Metallurgy Research building that was constructed in 1952. This new 20,000 ft^2 laboratory space will house several state-of-the-art instruments for small-scale synthesis and characterization of actinide materials. The large majority of the samples produced in this small-scale research lab will support various LDRD (Laboratory Directed Research and Development) projects as well as new and current programmatic activities, keeping LANL at the forefront of actinide research and holding the designation of being the Pu Center of Excellence.

Further reading:

1. *Los Alamos Science, Challenges in Plutonium Science, No. 26, 2000.*
2. *D.L. Clark, S.S. Hecker, G.D. Jarvinen, M.P. Neu, "The chemistry of the actinides and transactinides in plutonium," Chapter 7, Springer, 2006.*
3. *Integrated Plutonium Science and Research Strategy, LAUR-13-24336, Los Alamos National Laboratory, Lawrence Livermore National Laboratory.*
4. *E.D. Bauer, P.H. Tobash, J.N. Mitchell, J.L. Sarrao, "Single crystal growth of plutonium compounds from molten metal fluxes," Phil. Mag. 2012, 92, 2466.*
5. *E.D. Bauer, P.H. Tobash, et al. "Physical properties of plutonium intermetallic compounds," Ed., American Nuclear Society, Plutonium Handbook.*
6. *J. L. Sarrao, L.A. Morales, J.D. Thompson, B.L. Scott, G.R. Stewart, F. Wastin, J. Rebizant, P. Boulet, E. Colineau, G.H. Lander, "Plutonium-based superconductivity with a transition temperature above 18 K," Nature 2002, 420, 297.*
7. *E.D. Bauer, M.M. Altarawneh, P.H. Tobash, K. Gofryk, O.E. Ayala-Valenzuela, J.N. Mitchell, R.D. McDonald, C.H. Mielke, F. Ronning, J.-C. Griveau, E. Colineau, R. Eloirdi, R. Caciuffo, B.L. Scott, O. Janka, S.M. Kauzlarich, J.D. Thompson, "Localized 5f electrons in superconducting $PuCoIn_5$: consequences for superconductivity in $PuCoGa_5$," J. Phys.: Condens Matter 2012, 24, 052206.*
8. *D.W. Wheeler, R.F.E. Jenkins, R.K.B. Gover, M.B. Matthews, P. Roussel, "Structure and properties of a Pu–0.18 wt.% Ga alloy," J. Nucl. Mater. 2013, 440, 21.*
9. *D.W. Wheeler, S.M. Ennaceur, M.B.J. Matthews, "Phase stability of an aged Pu–0.27 wt.% Ga alloy," J. Nucl. Mater. 2015, 456, 68.*
10. *D.W. Wheeler, S.M. Ennaceur, M.B.J. Matthews, P. Roussel, P.D. Bayer, "Structure and phase stability of a Pu-0.32 wt% Ga alloy," J. Nucl. Mater. 2016, 476, 205.*
11. *D.W. Wheeler, S.M. Ennaceur, M.B.J. Matthews, P. Roussel, "Structure and phase stability of a Pu–0.42 wt.% Ga alloy," J. Nucl. Mater. 2014, 452, 509.*
12. *N. Harrison, J.B. Betts, M.R. Wartenbe, F.F. Balakirev, S. Richmond, M. Jaime, P.H. Tobash, "Phase stabilization by electronic entropy in plutonium," Nat. Commun. 2019, 10, 3159.*
13. *S. Rosen, M.V. Nevitt, A.W. Mitchell, "Metallographic and X-ray observations of Pu-C alloys," J. Nucl. Mat. 1963, 10, 90.*
14. *M. Drulis, "Low temperature heat capacity measurements of U_6FeH_{15} hydride," J. Alloys Compds. 1995, 219, 41.*

Acknowledgments

Many thanks to several individuals who contributed to this work both in the laboratory and/or through long discussions throughout the research projects. These include: Jeremy N. Mitchell, Eric D. Bauer, Scott Richmond, Franz Freibert, Daniel S. Schwartz, David W. Wheeler (AWE, UK), and Thomas E. Albrecht-Schmitt (Florida State University).

Daniel Rios

Daniel Rios is a Scientist at Los Alamos National Laboratory, New Mexico. He presented his talk titled "Identification of chlorine-containing gases in PuO_2 Storage Containers" *at Pu Futures 2018 in the Surface Science and Corrosion I technical session.*

Corrosion in Long-Term Storage Containers Packaged with Hydrated PuO_2/Salt Mixtures

Daniel Rios, Andrew J. Gaunt, Joshua E. Narlesky, John M. Berg, D. Kirk Veirs, Laura A. Worl

Los Alamos National Laboratory, Los Alamos, New Mexico 87545

Plutonium is a dynamic, unstable element that presents unique challenges for its safe long-term storage. The Department of Energy (DOE) stores excess plutonium-bearing materials in double-nested stainless steel containers (Fig. 1). The 3013 Standard (DOE-STD-3013), "Stabilization, Packaging, and Storage of Plutonium-Bearing Materials," defines the stabilization and packaging requirements that assure excess plutonium can be safely stored for 50 years. It specifies that storage containers be fabricated from corrosion-resistant materials such as 304L or 316L stainless steel. The 3013 Standard also requires both stabilization of the plutonium material prior to packaging to remove volatile components, and a moisture measurement after stabilization to confirm the moisture is less than 0.5 wt.%. A DOE-sponsored Surveillance and Monitoring Program (SMP) incorporates field non-destructive examinations (NDEs) and field-destructive examinations (DEs) to monitor the condition of in-service 3013 containers, including those enclosing hydrated PuO_2/salt mixtures.

Corrosion in stainless steel containers

Field-destructive examinations of 3013 containers have revealed corrosion in some containers packaged with hydrated PuO_2/salt mixtures (Fig. 2). Corrosion (general corrosion and pitting) occurred on both convenience (innermost container) and inner containers (CCs and ICs, respectively). Corrosion on the CCs was observed in both the contact region, the area where the bulk material is in contact with stainless steel, and in the headspace region, where there is no contact of the bulk material with stainless steel. Corrosion on the ICs was observed in the inner container closure weld region (ICCWR). This region is susceptible to stress corrosion cracking (SCC) due to the high residual stress from the weld process.

Energy-dispersive X-ray (EDX) analyses of corrosion deposits in the ICCWR showed the presence of chloride anions (Cl^-) but no metal cations from hydrated PuO_2/salt mixtures (e.g., Na, K, Ca, Mg, or Pu) that would indicate particulate transport of Cl^- to that location (Fig. 3). This suggests that Cl^- were transported from the material to the ICCWR via chlorine-containing gases (HCl or Cl_2). Once in the headspace, these chlorine-containing gases could adsorb onto the ICCWR surface and react, initiating pitting corrosion and SCC. The severity of such pitting corrosion and SCC is dependent on the chlorine-containing gas adsorbed. Chlorine-containing gases with higher redox potentials are more aggressive towards stainless steel (i.e., Cl_2 > HCl). Therefore, the aim of our work was to identify the chlorine-containing gases being emitted by the enclosed hydrated PuO_2/salt mixtures to better evaluate the risk for SCC in packaged 3013 containers.

Figure 1. The 3013 containers used by Hanford Site for long-term storage of plutonium-bearing materials. From left to right: outer, inner and convenience container

Figure 2. Corrosion observations at destructive examination (DE) of some 3013 containers packaged with hydrated PuO_2/salt mixtures. Headspace and contact region corrosion was observed on the inner (*left*) and convenience (*right*) containers, respectively.

Identification of gases emitted by hydrated PuO_2/salt mixtures

Hydrated PuO_2/salt mixtures were prepared by mixing PuO_2 with anhydrous $CaCl_2$ or $MgCl_2$ and heating the mixtures at 800°C for two hours under a helium atmosphere. The PuO_2/salt mixtures were then placed inside an enclosed humidified balance for water addition by vapor diffusion.

HCl and Cl_2 gases were captured by exposing the solid alkenes 4-(dimethylamino)stilbene (DMAS) and trans-stilbene, respectively, to the headspace gas above hydrated PuO_2/salt mixtures. Capture of HCl gas occurred by an acid-base reaction between HCl gas and the dimethylamino group in DMAS, giving DMAS-hydrochloride. Capture of Cl_2 gas occurred by chlorination of the olefinic double bond in trans-stilbene. Identification of protonated and chlorinated solid alkenes was achieved using NMR spectroscopy.

A carbon steel sample was exposed to the headspace gas above a hydrated PuO_2/salt mixture. This type of steel, which has more carbon than stainless, was chosen to accelerate the reactions. Corrosion was observed on the specimen within a few days; a photograph was taken after 50 days (Fig. 4). The exposure was performed but a carbon steel specimen was used in place of solid alkenes. These experiments clearly show that the headspace gas above hydrated PuO_2/salt mixtures is corrosive and that HCl and Cl_2 gases are present.

Capture mechanism of HCl and Cl_2 gases by alkenes

We can use the chemistry that occurs between alkenes and chlorine-containing gases to selectively choose the type of alkene to allow discriminatory identification of HCl, Cl_2 or both gases. Capture of chlorine-containing gases is known to occur via addition reactions with olefinic double bonds of alkene compounds. These reactions can occur in both solution and gas-solid states. Capture of gaseous HCl by an alkene in solution occurs via electrophilic addition of HCl to the alkene double bond in a two-step mechanism. In the first step, the electrophile (H^+) adds to the olefinic double bond forming the most stable carbocation. The nucleophile (Cl^-) then attacks the carbocation to generate the product.

Capture of gaseous HCl by a solid alkene occurs via both electrophilic addition and acid-base reaction (if there is an amino group present on the alkene). Capture of gaseous Cl_2 by an alkene in solution meanwhile occurs via syn- or anti-addition of Cl_2 to the alkene double bond. In syn-addition, the two Cl atoms in Cl_2 add to the same face of the olefinic double bond, whereas in anti-addition, the two Cl atoms add to opposite faces of the double bond. Capture of Cl_2 gas by solid alkenes occurs via both syn- and anti-additions.

Discussion of corrosion chemistry

Generation of HCl and Cl_2 gases from hydrated PuO_2/salt mixtures can be attributed to radiolysis of $MCl_2(H_2O)_x$ (M = Ca, Mg) salts and/or secondary chemical reactions. Hydrolysis is an unlikely mechanism due to the temperatures (~25°C) at which the present study was performed—generation of HCl gas by hydrolysis of $MCl_2(H_2O)_x$ has been shown to require elevated temperatures.

Radiolysis of salts can lead to the generation of chlorine radicals (Cl•). Two chlorine radicals can associate to form chlorine gas, Cl_2 (Eqn. 1), which can diffuse into the headspace of the irradiated salt crystals. Alternatively, the chlorine radical could associate with a chloride anion and form a radical-anion, $Cl_2^{\bullet-}$, which can disproportionate to generate chlorine gas (Eqn. 2).

(1) $Cl\bullet + Cl\bullet \longrightarrow Cl_2$

(2) $Cl\bullet + Cl^- \longrightarrow Cl_2^{\bullet-} \longrightarrow \frac{1}{2} Cl_2 + Cl^-$

HCl gas may be generated by radiolysis and/or by secondary chemical reactions. In a radiolysis mechanism, HCl can form by reactions between hydrogen and chlorine radicals (Eqn. 3); the hydrogen radicals are products from water radiolysis (Eqn. 4) occurring in the hydrated PuO_2/salt mixtures. Alternatively, HCl may be generated by secondary chemical reactions between radiolytically-derived Cl_2 and background H_2O gases (Eqn. 5).

(3) $H\bullet + Cl\bullet \longrightarrow HCl$

(4) $H_2O \longrightarrow e^-_{aq}, OH\bullet, H\bullet, H_2O_2, H_2, H^+$

(5) $Cl_2 + H_2O \longrightarrow HCl + HClO$

Previous experiments did not have the capabilities to capture radiolytic chlorine-containing gases present in the headspace of irradiated salts. The techniques (e.g., mass spectrometry) applied in such experiments were not suitable for the identification of these gases as they are extremely reactive with other headspace gases and metal surfaces. In such previous experiments, radiolytically-derived Cl_2, trapped within irradiated salt crystals, was identified by dissolving the irradiated salt in water and photometrically measuring the hypochlorite (ClO^-) concentration.

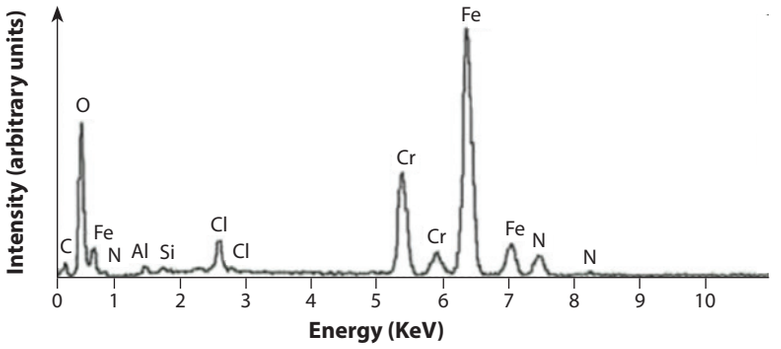

Figure 3. Energy-dispersive X-ray (EDX) spectrum of the corrosion products associated with a pit on the inner container closure weld region (ICCWR). The spectrum shows the presence of chloride and the absence of cations like K, Na, Ca, Mg, or Pu that are associated with chloride in 3013 containers.

Summary

This study shows that the headspace gas above hydrated PuO_2/salt mixtures is sufficiently corrosive to oxidize a carbon steel coupon, and presumably stainless steel, as deduced from our field-destructive tests. Although stainless steel is corrosion-resistant under environmental conditions, it can be attacked when corrosive gases (e.g., HCl, Cl_2), H_2O, and O_2 are present, which have been identified in the headspace above hydrated PuO_2/salt mixtures. This suggests the headspace gas above similar mixtures packaged in 3013 containers contains HCl and Cl_2 gases, and that these gases together with O_2 and H_2O cause the corrosion observed when stored containers have been opened and examined. None of the containers we have tested have shown through-wall corrosion—only surface corrosion and minor pitting have been observed so far. Storing the material dry would prevent the generation of corrosive gases, O_2, H_2O, and thus prevent corrosion in containers.

The insights from the present study, in conjunction with future planned studies, are intended to move towards a comprehensive understanding of corrosive gas generation over time for different plutonium-bearing materials. The results will ultimately underpin a science-driven safety basis for effectively monitoring and managing long-term storage of these materials.

Figure 4. Corrosion observed on a carbon steel specimen exposed to the headspace gas above a hydrated PuO_2/salt mixture for 50 days.

Acknowledgments

The author thanks the Department of Energy–Savannah River (DOE-EM) for funding of this work. The author also gratefully acknowledges the work of the Surveillance and Monitoring Program corrosion-working group (CWG) and technicians involved in this project: Edward L. Romero, Kennard V. Wilson, Brian B. Sandoval, Michael Ramos, and Michael D. Greenbank.

Plutonium Handbook Second Ed. co-authors at Pu Futures 2018

Plutonium Handbook Second Ed. editorial team

Some of the authors at Pu Futures 2018

The effort to update the fifity-year-old Plutonium Handbook began at Pu Futures 2010 in Keystone, CO. After much discussion, encouraged by Siegfried Hecker, the team of Clark, Geeson, and Hanrahan committed to produce a scholarly update to this classic reference.

Fittingly, the international team of technical authors and editors of the second edition met at Pu Futures 2018 in San Diego, CA to finalize details of the much-awaited update to this indispensible actinide science resource.

Plutonium Handbook Second Edition

EDITORS

DAVID L. CLARK
LOS ALAMOS NATIONAL LABORATORY, USA

DAVID A. GEESON
ATOMIC WEAPONS ESTABLISHMENT, UK

ROBERT J. HANRAHAN, JR.
NATIONAL NUCLEAR SECURITY ADMINISTRATION, USA

ABOUT

Fifty years after publication of the original Plutonium Handbook, this timely and authoritative second edition provides unparalleled coverage of plutonium research. Topics include:

- history of the discovery of plutonium
- properties of plutonium isotopes
- chemistry and properties of plutonium metal and alloys
- plutonium in nuclear fuels, waste forms, and heat sources
- packaging, storing, and transportation of plutonium
- plutonium aging
- nuclear security and safeguards
- thermodynamic trends of plutonium
- techniques for working with plutonium

This edition comprises 87 articles (3733 pages) supported by contributions of 215 authors from 13 countries, a truly international collaboration which brings together an entire community of researchers from academia, national laboratories, and research institutions. The Plutonium Handbook Second Edition is expertly produced and will be a mainstay for future generations.

A significant addition to the handbook is a volume dedicated to the techniques for encapsulation and safe handling of radioactive materials, which are covered for the first time. Most techniques that have been applied to the study of plutonium and appear in the literature are covered in this volume.

RELEASE

Available fall 2019 from the American Nuclear Society.

ans.org/pu

Los Alamos NATIONAL LABORATORY EST.1943

Amy Hixon

Amy Hixon is an Assistant Professor at the University of Notre Dame, Indiana. She presented her invited talk titled "Plutonium Environmental Chemistry: Mechanisms for the Surface-Mediated Reduction of Pu(V/VI)" *at Pu Futures 2018 in the Solution and Gas Phase Chemistry I technical session.*

Plutonium Reduction at the Solid-Water Interface

Amy E. Hixon
Civil & Environmental Engineering & Earth Sciences, University of Notre Dame, Indiana

The actinide elements, including plutonium, carry great societal importance due to their use in medicine, power generation, and national security, but present a risk to human health and the environment due to their high toxicity and long half-lives. Although there is a global consensus that geologic disposal is the safest existing approach to dealing with used nuclear fuel and high-level nuclear waste, only a few nations are moving towards implementing a geologic repository due to technical and political barriers. Understanding the factors that affect the mobility of plutonium in the subsurface environment is critical to support the development of such repositories and will be essential for remediating locations contaminated as a result of nuclear weapons production and testing.

Overview of plutonium geochemistry

Plutonium is unique among the transuranic elements in that it can simultaneously exist as tri-, tetra-, penta-, and hexavalent oxidation states (i.e., 3+ to 6+, or III—VI in Roman numeral form) in a single solution. This ability to exist in multiple oxidation states stems from similarities in reduction potentials across the pH range, which results in a high sensitivity of plutonium oxidation state to changes in pH or reduction potential of the system. The importance of oxidation-reduction (redox) chemistry in determining plutonium mobility cannot be overstated. While tetravalent Pu^{IV} is generally assumed to be immobile in the subsurface environment due to sorption or precipitation, pentavalent Pu^{V} tends to be mobile due to its relatively low effective charge and weak complex formation. Consistent with these assumptions, recent research has shown that in a mineral-water system at equilibrium, plutonium in the aqueous phase is found as Pu^{V}, whereas Pu^{IV} is associated with the mineral.

Plutonium speciation and complexation also influence the behavior of plutonium at the mineral-water interface. The oxidized forms of plutonium are found as the near-linear plutonyl cations $Pu^{V}O_2^{+}$ and $Pu^{VI}O_2^{2+}$, which resist hydrolysis until alkaline conditions are reached. Conversely, the reduced forms of plutonium exist as hydrated cations (i.e., Pu^{3+}, Pu^{4+}), hydrolyze even under acidic conditions, and can form insoluble hydroxides, particularly under high plutonium concentrations. Under slightly alkaline conditions, plutonium-carbonate complexation is favored over hydrolysis. In contrast to the positively-charged or neutral plutonium hydrolysis species, the tetra- and pentavalent Pu-carbonate aqueous complexes are almost exclusively negatively charged. Therefore, the presence of carbonate results in a significant change in aqueous plutonium speciation that may affect plutonium sorption to negatively-charged mineral surfaces.

(a) Reduction via electron shuttling

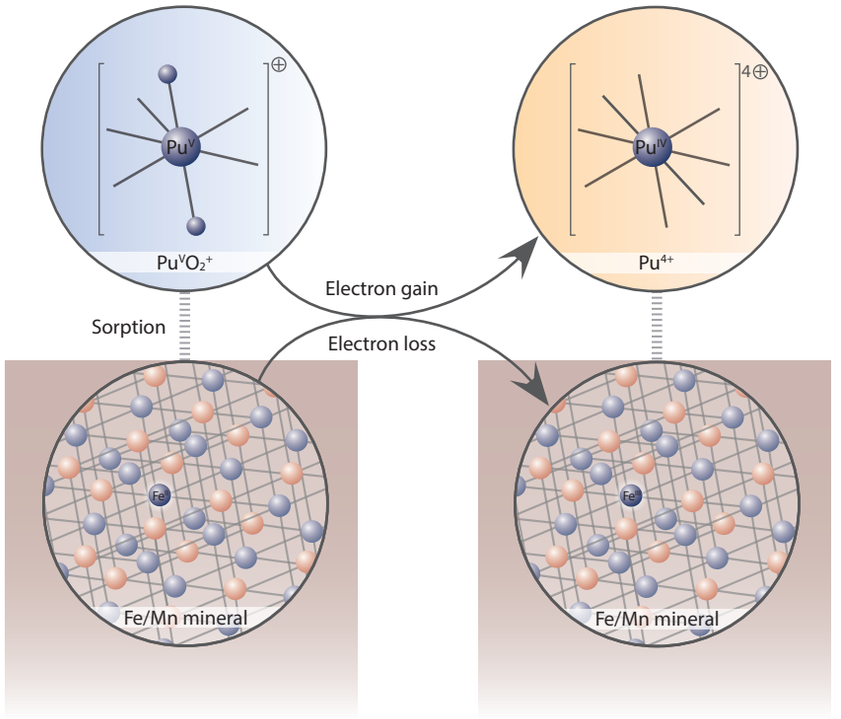

(b) Reduction via thermodynamic favorability

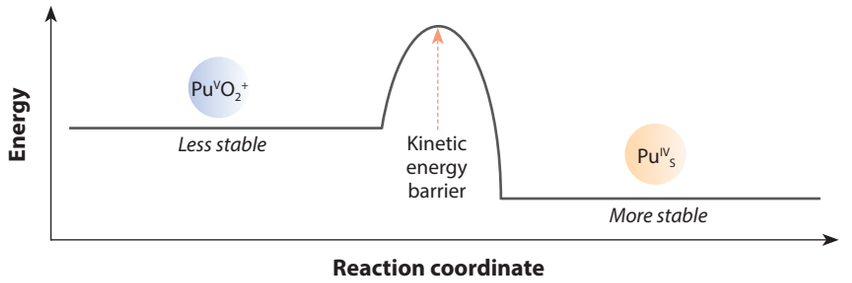

Figure 1. The oxidation state of plutonium dictates its mobility in the environment. These schemes show possible types of plutonium reduction (electron gain, decrease in oxidation state) at the solid-water interface of pure minerals and native soils: (a) Electron shuttling process which involves sorption of the Pu^{V} ions directly to semiconducting minerals which can supply ("shuttle") electrons in their supramolecular lattice; (b) Thermodynamic favorability of Pu^{IV} surface complexes or colloids Pu^{IV}_{S} over aqueous Pu^{V} complexes, which explains plutonium reduction on materials which cannot shuttle electrons.

Plutonium is particularly susceptible to disproportionation, a specific type of redox reaction in which electron transfer occurs; a proportion of the ions are reduced and another portion are oxidized without water or other elements acting as electron shuttles. As shown below, Rxn. 1 describes the disproportionation of Pu^{V}:

(1) $$2Pu^{V}O_2^{+} + 4H^{+} \rightleftharpoons Pu^{4+} + Pu^{VI}O_2^{2+} + 2H_2O$$

Analysis of this reaction shows that disproportionation will increase as the plutonium concentration increases. Furthermore, we can deduce that as the pH of the system is raised, the disproportionation of Pu^{V} becomes less important. It is important to note that the seminal works establishing plutonium disproportionation were conducted at pH 0 and therefore do not take into consideration the effect of hydrolysis on the disproportionation reaction as the pH is raised. The extrapolation of this effect is currently unknown.

The sorption of plutonium ions and complexes to soils, sediments, and pure minerals is of interest because these interactions have the potential to immobilize plutonium and therefore minimize the impact to human health. This short overview highlights one important aspect of plutonium behavior at the mineral-water interface—the concept of surface-mediated reduction, which describes the reduction of plutonium on a mineral surface.

Plutonium reduction at the solid-water interface

Numerous laboratory studies have observed the capacity of pure minerals and native soils to reduce plutonium, which is typically added to the aqueous phase as Pu^{V}. In some studies, reduction of plutonium is measured directly through the use of spectroscopic techniques, such as X-ray absorption spectroscopy (XAS), whereas in other studies indirect methods, such as solvent extraction, are used. In all cases in which the aqueous-phase oxidation state is measured, no Pu^{IV} is present. Therefore, reduction occurs at or near the mineral surface and not in the bulk aqueous phase. Despite these studies, the exact mechanism(s) responsible for surface-mediated redox reactions remain unclear. There are several hypotheses for the surface-mediated reduction of plutonium under environmental conditions:

- Surface precipitation
- Electron transfer or electron shuttling
- Thermodynamic favorability
- *Radiolysis at the mineral surface* *
- *Disproportionation of Pu^{V}* *

* disproved

Of these, radiolysis at the mineral surface and disproportionation of Pu^{V} have been disproven (see Further Reading), so we will focus on some of the evidence supporting the remaining hypotheses in the discussion below.

Surface precipitation

The exact mechanism of complex formation depends upon the plutonium:mineral ratio and the total plutonium concentration. We usually assume, and geochemical models generally predict, the formation of monomeric surface species. However, when the plutonium concentration is greater than a certain value, precipitates or polymeric colloids may form. The plutonium concentration at which surface complexes shift from monomeric to polymeric is not well constrained, but is believed to be around 10^{-9} to 10^{-7} M, depending upon the mineral surface(s) present. The solubility-limiting phase is also not well constrained, but is generally attributed to the Pu^{IV} hydrous oxide—PuO_{2+x}(s, hyd)—also known as the intrinsic plutonium oxide colloid or plutonium polymer. An interesting point to note is that all of the surface precipitates identified thus far in the literature contain Pu^{IV}, which requires the reduction of Pu^{V}. The driver for this is usually explained using thermodynamics, described below.

The development of field-scale models describing plutonium transport in the environment will need to consider both near- and far-field environments (i.e., close to or far from the source term). Under near-field conditions, we can expect—among other things—high plutonium concentrations. Therefore, surface precipitation may be a particularly important driver for plutonium surface-mediated reduction under these conditions. Currently available peer-reviewed studies primarily focus on iron oxide minerals and use high-resolution transmission electron microscopy (HRTEM) and XAS to show the formation or association of plutonium nanoparticles at mineral surfaces. In some cases, lattice distortion occurs, which may be indicative of stronger binding of plutonium compared to systems in which distortion is not observed.

Electron transfer or electron shuttling

The elements iron and manganese are important not only for the subsurface transport of plutonium, but are also an integral part of defining the types and amounts of radioactive material that will be released to the environment under a variety of geologic repository concepts. Iron is ubiquitous in the subsurface environment in the form of iron minerals, which exist in oxidized (e.g., hematite α-$Fe^{III}_2O_3$ and goethite α-$Fe^{III}OOH$), mixed-valent (e.g., magnetite $Fe^{II}(Fe^{III})_2O_4$), and reduced (e.g., pyrite $Fe^{II}S_2$, siderite $Fe^{II}CO_3$) forms, and as a trace constituent of other mineral phases, such as smectite clays. In fact, nuclear waste repository designs strategically introduce large amounts of reduced iron (Fe^0) in order to stabilize the lower oxidation states of plutonium. Although less abundant than iron, manganese is also prevalent in the environment in forms such as pyrolusite ($Mn^{IV}O_2$), manganite ($Mn^{III}OOH$), cryptomelane ($K(Mn^{IV}_7Mn^{III})O_{16}$), and hausmannite ($Mn^{II}(Mn^{III})_2O_4$). The iron and manganese in these minerals support electron transfer and electron shuttling processes.

Electron transfer is the process by which an electron moves from one atom or molecule to another (Fig. 1a). In order for electron transfer to occur at the solid-water interface, plutonium must sorb directly to an Fe^{II}-, Mn^{II}-, or Mn^{III}-bearing surface site. Fe^{II}, Mn^{II}, or Mn^{III} will lose electrons (oxidation) and Pu will gain electrons (reduction). Arthur Sanchez of the University of Washington was the first to propose that trace amounts of Fe^{II} present at the goethite surface may be responsible for the surface-mediated reduction of Pu^V in an article titled "The adsorption of plutonium IV and V on goethite," which was published in Geochimica et Cosmochimica Acta in 1985. More recent work on treated and untreated sediments from the Savannah River Site support his hypothesis, however there are several examples in the literature which show that the mere presence of Fe^{II} cannot always completely account for observed plutonium sorption behavior.

Iron and manganese oxide minerals are semiconductors, meaning that the valence electrons in these minerals are free to move between atoms in the crystal's conduction band. The ease with which electrons from the valence band are promoted to the conduction band is based on the energy of the band gap separating the valence and conduction bands. In some cases, exposure to sunlight may be sufficient to promote electrons from the valence band to the conduction band. Thus, Pu^V does not have to sorb directly onto an Fe^{II}- or Mn^{II}-bearing site since electrons can be shuttled through the bulk mineral. This mechanism is supported by an observed increase in the rate of Pu^V sorption with increasing light intensity and an increase in the sorption of Pu^V to marine sediments with decreasing wavelength.

Thermodynamic favorability

The thermodynamic favorability of Pu^{IV} surface complexes or colloids explains observations of plutonium reduction on mineral surfaces that are not semiconductors and do not contain impurities that can act as electron shuttles (Fig. 1b). Examples include quartz and amorphous silica. The basis of the conceptual model is that a Pu^{IV} hydroxide surface complex or Pu^{IV} precipitate is more energetically favored than an aqueous Pu^V complex. Some calculations suggest that the redox potential of the Pu^V/Pu^{IV} couple would only need to be raised by 0.28 V in order for this model to be valid. Therefore, the formation of a surface-bound, hydrolyzed Pu^{IV} complex or Pu^{IV} colloid could drive the reduction of Pu^V to Pu^{IV}.

Of all the hypotheses for the surface-mediated reduction of plutonium, the thermodynamic favorability of tetravalent Pu surface complexes or colloids offers the greatest opportunity for future research, as the redox potential of the Pu^{V}/Pu^{IV} couple has not been measured in the presence of a mineral surface and currently there is no obvious method of proving the hypothesis to be true. Considering the known thermodynamic favorability of tetravalent Pu-hydroxide complexes and the abundant hydroxide sites on mineral surfaces, the possibility of the increased reduction potential of a surface complex as compared to the aqueous redox potential should be examined further.

Summary

The reduction of penta- to tetravalent Pu at the solid-water interface can minimize the mobility of plutonium in the subsurface environment. It is likely that several factors contribute to the surface-mediated reduction of plutonium and that these factors may vary depending upon the composition of the solid phase. A review of the literature shows that of the proposed hypotheses for the surface-mediated reduction of plutonium, two have been disproven (radiolysis and disproportionation), one is likely (electron transfer or shuttling), and two warrant further research (surface precipitation and thermodynamic favorability). While currently-existing spectroscopic techniques will be useful for probing the surface-mediated redox mechanisms occurring in the near-field environment of a geologic repository, plutonium concentrations in the far-field environment are significantly lower and present a major analytical challenge in order to avoid potentially costly and inaccurate extrapolations. Advances in trace- and ultra-trace-level methodologies are needed so that such studies can produce accurate and reliable results.

Further reading:

1. *A.E. Hixon, Y. Arai, B.A. Powell, "Examination of the effect of alpha radiolysis on plutonium(V) sorption to quartz using multiple plutonium isotopes," J. Colloid Interface Sci. 2013, 403, 105.*
2. *A.E. Hixon, B.A. Powell, "Observed changes in the mechanism and rates of Pu(V) reduction on hematite as a function of total plutonium concentration," Environ. Sci. Technol. 2014, 48, 9255.*
3. *A.E. Hixon, B.A. Powell, "Plutonium environmental chemistry: Mechanisms for the surface-mediated reduction of Pu(V/VI)," Environ. Sci.: Process. Impacts 2018, 20, 1306.*
4. *D. Shaughnessy, H. Nitsche, C.H. Booth, D.K. Shuh, G.A. Waychunas, R.E. Wilson, H. Gill, K.J. Cantrell, R.J. Serne, "Molecular interfacial reactions between Pu(VI) and manganese oxide minerals manganite and hausmannite," Environ. Sci. Technol. 2003, 37, 3367.*

Searching for Zero Plutonium in the Far North of Scotland

Malcolm J Joyce,[1] Chris Tighe,[1] Marcus Christl,[2] Maxi Castrillejo,[2] Claude Degueldre,[1] Kirk Semple,[1] Jeremy Andrew[3]

Plutonium in the natural environment is often assumed to be extinct since the half-lives of most of its isotopes are short relative to the age of the Earth. Indeed, uranium has historically been considered the heaviest naturally-occurring element. However, as Levine and Seaborg reported in the Journal of the American Chemical Society in 1951, this has long been known not to be the case. Albeit in excruciatingly miniscule quantities, Seaborg and Levine reported the possibility that ^{239}Pu might form naturally, via neutron capture on ^{238}U with neutrons derived from spontaneous fission and (α, n) reactions on light isotopes stimulated by the same. This rendered quantities measurable with alpha spectroscopy in the Canadian pitchblende Levine and Seaborg probed some 10 years after element-94 was discovered.

Few would regard an abundance of plutonium in the ground anything too far from zero as desirable, particularly given the critical role of soils in food production. Indeed, as Pszonicki et al. remark in their International Atomic Energy Agency (IAEA) inter-comparison of 1984, "…the concentration of radionuclides should be checked periodically, especially in industrial areas." However, for environmental protection agencies and regulators, the question can be more complex, i.e., given that the abundance in soils is not zero, what is it and at what point does the contribution from mankind's activities in the last 80 years necessitate its clean-up?

Our aim is to answer this question for plutonium in the natural environment in the United Kingdom, with a focus on the Dounreay Fast Reactor site in the far north of Scotland. The benefit of this research is that it helps quantify the anthropogenic contribution borne of reactor activities to the abundance in this specific locale. Furthermore, it may determine whether specific isotopic signatures might help pinpoint material originating from reactor operations.

In addition to the natural processes described above, plutonium arises in the environment from a variety of anthropogenic sources. These include: nuclear reactor accidents, the accidental loss on launch or the re-entry and burn-up of radioisotope thermionic generators (RTGs) from satellites, the accidental loss and dispersion of material from nuclear weapons, nuclear weapon detonations and tests, and the dispersion of effluents from nuclear reprocessing facilities. These sources are often further delineated as to whether they are global, i.e., nuclear weapon detonations and tests, or localized (effluents and the result of accidents). A plutonium assay of localized sources is desirable to distinguish it from global fallout, as John H. Harley suggested in the Journal of Radiation Research in 1980.

[1] Lancaster University, United Kingdom; [2] ETH Zürich, Switzerland; [3] Dounreay Site Restoration Limited (DSRL), Dounreay, Scotland.

Malcolm J Joyce

Malcolm Joyce is a Professor and Royal Society Wolfson Research Merit Award Holder at Lancaster University, UK. He presented his talk titled "A comparison of plutonium abundance in soil from sites in the United Kingdom measured with high efficiency, high-resolution gamma-ray spectroscopy, neutron assay and accelerator mass spectrometry" *at Pu Futures 2018 in the Environmental Chemistry II technical session.*

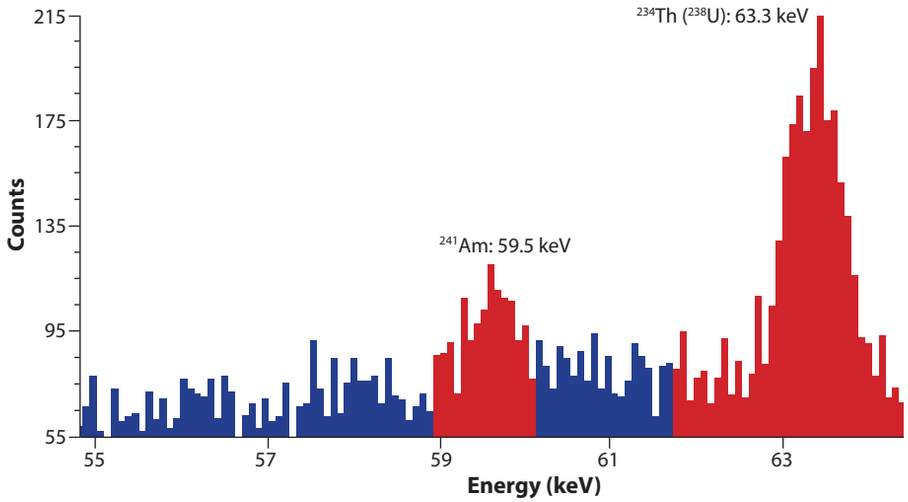

Figure 1. A section from a gamma ray spectrum taken with the BEGe counter, showing the ^{241}Am line at 59.5 keV and the 63.3 keV line from the ^{234}Th daughter of ^{238}U.

Assay methodology

The established method for plutonium assay in the environment is alpha spectroscopy, utilizing alpha decay in the majority of prevalent plutonium isotopes. However, this can require extensive sample processing and refinement to obtain sufficiently active products of environmental samples, and trace quantities can require long counting times with limited isotopic separation. By contrast, accelerator mass spectrometry (AMS) yields highly sensitive mass estimates relative to a known spike (usually ^{242}Pu) and isotopic ratios, inter alia, ^{240}Pu/^{239}Pu, ^{241}Pu/^{239}Pu, etc. The latter can identify the origin of the plutonium residue under scrutiny due to differences that arise in the mechanism by which it was formed; for this reason, we aimed to measure the abundance of more than one isotope of Pu (in this work, ^{239}Pu and ^{241}Pu).

Inherent neutron emission (such as spontaneous fission in ^{240}Pu) is rarely strong enough in environmental samples to be exploited in a trace assay. However, direct gamma-ray spectrometry benefits from a technology base that is arguably more mature and, furthermore, shows decay transitions with sufficient intensity to support an estimate of isotopic abundance. In comparison with the assay of nuclear fuel samples, many of the lines corresponding to a spectrum recommended in the literature (c.f., the Passive Non-Destructive Assay—PANDA—manual) are not prominent for trace analysis in environmental samples because the dispersed quantities are too small. In our samples, the 129.3 keV line in ^{239}Pu is contaminated by a prominent decay in ^{228}Ac (itself derived from frequently-abundant ^{232}Th), while the 148.6 keV (^{241}Pu) and 152.7 keV (^{238}Pu) lines are weak because the abundance of these isotopes is low. This leaves the 59.5 keV line from ^{241}Am with which to infer ^{241}Pu (assuming the residue is aged long enough for the decay from ^{241}Pu to occur) and that the age of the trace plutonium can be estimated (Fig. 1).

Measurements on soil samples

We studied soil samples from sites in the UK, chosen due to their distance from the site of interest and the relative lack of disturbance they had been subject to:

- 10 samples on-site, Dounreay in Caithness, Scotland
- 2 samples off-site, but nearby
- 2 samples far-from-site, ~350 miles south in Yorkshire and Derbyshire

In order to determine ^{241}Pu and ^{239}Pu abundances we used gamma-ray spectrometry with a broad energy germanium (BEGe) counter, and a TANDY accelerator mass spectrometry (AMS) system, respectively (Fig. 2).

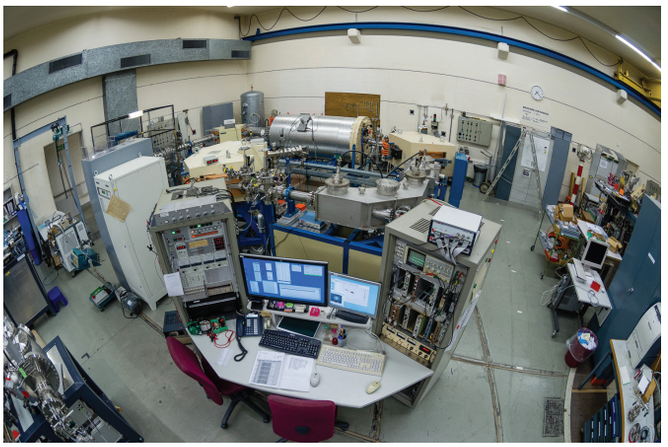

Figure 2. *Left*: The TANDY accelerator mass spectrometry (AMS) setup at ETH Zürich, Switzerland, for determining ^{239}Pu abundances. *Right*: The BEGe counter at the Culham Centre for Fusion Energy (CCFE), Abingdon, UK, for determining ^{241}Pu abundances.

A diversity of plutonium abundance measurements have been reported from all over the world in the last 65 years. The abundance in the northern hemisphere is higher than that in southern hemisphere because the majority of nuclear weapons tests (and thus atmospheric pollution) took place in the north. Levine and Seaborg reported 550 fg/g for ^{239}Pu in 1951 in uranium ore deposits but cautioned as to the efficiency with which their extraction was able to yield all the plutonium present; this is still a concern today because aggressive dissolution can be necessary to extract all of the plutonium (note that a femtogram, fg, is 10^{-15} grams; 1 fg/g is equivalent to 1 part-per-quadrillion, ppq). Nonetheless, estimates for ^{239}Pu vary from the mid-thousands fg/g, for uranium deposits such as those at Cigar Lake, through to ~15 fg/g for samples from the North Pacific.

Plutonium-239 measurements

Our ^{239}Pu measurements are consistent with Levine and Seaborg's estimate (noting theirs was derived via alpha spectrometry; we used AMS) and fall in the middle of the range reported by Harley and which is adopted widely as world fallout levels. However, our measurements are consistently higher than those reports for which it is known fallout plays a smaller part, particularly those studies of lakes and oceans. The variation across the local samples in this research reflects a difference between those samples in the Dounreay vicinity and those far-from-site (the latter for example is ~380 fg/g). However, it is not clear whether this is evidence for dispersion of miniscule quantities of material from legacy activities on-site, the action of neutron capture in the relatively rich uranium deposits in the Dounreay region, or due to more significant pollution as a result of weapons tests or Chernobyl, since the site is of a more northerly latitude than the far-from-site samples. With regard to uranium abundance in the area, levels in excess of 1000 ppm were reported in alluvial deposits by the British Geological Society in volume 21 of Earthwise in 2004, for example, relative to ~5 ppm in Derbyshire where one of our far-from-site samples was derived.

Plutonium-241 measurements

Our ^{241}Pu data exhibit a trend similar to our ^{239}Pu data: the on-site samples are consistent with one another for both data sets, but the levels measured for the off-site and far-from-site samples contrast with each other (Fig. 3a). For example, we observe more ^{241}Pu in the off-site samples than in the on-site cases, while the situation for ^{239}Pu is reversed. This is not understood at present, but the on-site levels are consistent with far-from-site levels, suggesting a stronger association with fallout; the off-site samples may have been subject to greater disturbance as a result of building developments than the places from which samples were taken on-site since reactor operations ceased in 1994.

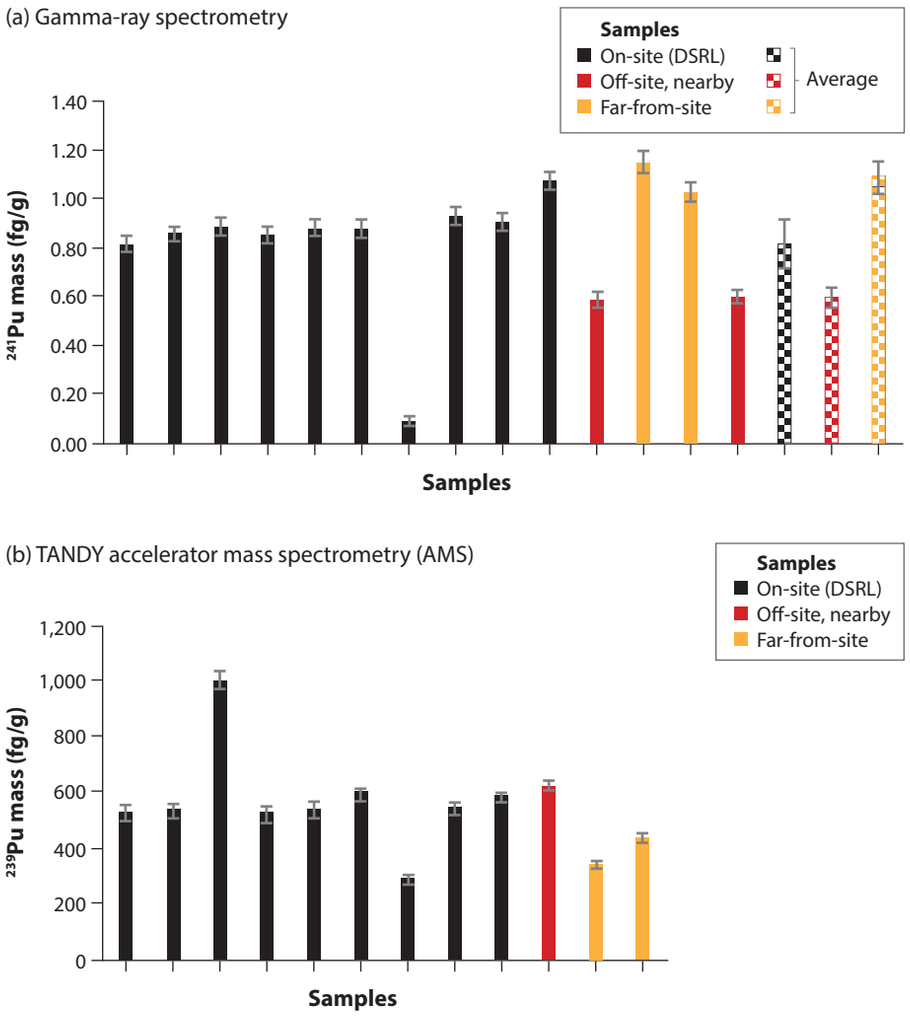

Figure 3. These graphs depict qualitatively consistent results with general expectations for the ^{241}Pu and ^{239}Pu isotopic abundances, derived from two complementary analytical methods: (a) ^{241}Pu abundance derived from gamma-ray spectrometry measurements; (b) ^{239}Pu data from AMS measurements, expressed in fg/g as a function of sample. [Black = on-site samples (DSRL, Dounreay Site Restoration Ltd.); red = off-site, nearby; yellow = far-from-site.]

A comparison of these data in Table 1 also yields estimates for the ^{241}Pu/^{239,240}Pu activity for the samples on-site, off-site, and far-from-site, respectively. Recourse to the literature (for example Corcho Alvarado et al. in their 2011 Radiochimica Acta work) suggests that ^{241}Pu/^{239,240}Pu ratios in European alpine soils are found in the range 0.8–3.0, dependent on the terrain and depth from which the sample is derived. They associate this with fallout from nuclear weapons tests because the ^{241}Pu component is small relative to what it would be from a reactor accident such as Chernobyl. Therefore, we draw the same conclusion. The absence of a ^{240}Pu assessment in our work thus far does not appear at odds with this outcome. Our abundance estimates for ^{241}Pu correspond to the range 2–4 Bq/kg, consistent with the lower range of the alpine measurements. These data were associated with wetland locations perhaps not dissimilar the coastal region of Caithness from which our on-site and off-site samples were derived.

Summary

This article illustrates the benefit that a combination of highly sensitive techniques can bring to the challenging area of trace plutonium assay in the environment. In the future we hope to acquire AMS data for ^{241}Pu to enable a direct comparison with our gamma-ray spectrometry data presented here and obtain an estimate of the age of the material, and additionally for ^{244}Pu—the latter is long-lived and only produced in significant quantities in nuclear detonations.

Table 1. A comparison of activity ratios from this research and that presented by Corcho Alvarado et al. in their Radiochimica Acta work of 2011.

Location	$^{241}Pu/^{239,240}Pu$ (this work)	$^{241}Pu/^{239,240}Pu$ (Corcho Alvarado et al.)
On-site	1.8±0.1	0.8 → 1.6* (dependent on terrain and depth) Valley of Piora, Switzerland
Off-site	2.1±0.1	1.1 → 3.0* Valley of Mercantour, France
Far-from-site	1.61±0.08	

* Typical uncertainty ±0.2

Hence, it will enable the fallout component to be isolated from local contributions. A further tell-tale which we hope to explore regarding the origin of the material is the $^{240}Pu/^{239}Pu$ ratio.

It remains singularly impressive that trace levels of plutonium of the order of parts-per-trillion can be discerned with relative ease in the laboratory, and in the case of direct gamma-ray spectrometry extensive sample preparation is no longer necessary. Harley likened the trace assay task to finding "…a penny in the US national debt"—this remains a reasonable analogy despite changes that have occurred since their seminal review nearly 40 years ago. We can therefore be confident that, while not zero, techniques exist with breath-taking sensitivity to quantify the trace residues of this infamous element in the natural environment.

Acknowledgments

We would like to acknowledge the support of Dounreay Site Restoration Ltd. (DSRL), the Engineering and Physical Sciences Research Council via grant number EP/R026084/1 and the Royal Society via a Wolfson Research Merit Award held by the author, M. J. Joyce. This research constitutes part of the material submitted for the degree of PhD by C. Tighe.

Further reading:

1. *J.A. Corcho-Alvarado, F. Chawla, P. Froidevaux, "Determining ^{241}Pu in environmental samples: Case studies in alpine soils," Radiochim. Acta 2011, 99, 121.*
2. *L. Pszonicki, A. N. Hanna, O. Suschny, "Report on intercomparison IAEA/SOIL-6 of the determination of Cs-137, Pu-239, Ra-226, and Sr-90 in soil," International Atomic Energy Agency, Vienna, 1984.*
3. *C.A. Levine, G.T. Seaborg, "The occurrence of plutonium in nature," J. Am. Chem. Soc. 1951, 73, 3278.*
4. *J. Harley, "Plutonium in the environment–a review," J. Rad. Research 1980, 21, 83.*
5. *D. Reilly, N. Ensslin, H. Smith, Jr., "Passive non-destructive assay of nuclear materials," Office of Nuclear Regulatory Research 1991.*

Per Söderlind

Per Söderlind is a Scientist at Lawrence Livermore National Laboratory, California. He presented his talk titled "Free-energy calculations for plutonium" *at Pu Futures 2018 in the Condensed Matter Physics II technical session.*

Free-Energy Calculations for Plutonium

Per Söderlind, Babak Sadigh
Lawrence Livermore National Laboratory, P.O. Box 808, Livermore, California 94550

Plutonium metal's unusual properties, reflected in part by its unique phase diagram, have in recent years been modeled typically using either density-functional theory (DFT) or +U methods that include local-density approximation and Hubbard U (LDA+U) and dynamical mean-field theory (DMFT). In these calculations, applying a large effective Hubbard U parameter indicates strong 5f-electron correlation that leads to localization (the U parameter tends to prevent movement of electrons between atoms) while the weaker correlations included within DFT cause delocalization of the 5f electrons. In the +U approaches for plutonium it was decided long ago to use a large value of U (> 4 eV), a choice that has remained popular up until recently which has also been applied to the localized 5f electrons in americium metal. These two views on the physics of plutonium have been debated vigorously.

It now appears that the weaker electron-correlation picture has been confirmed, surprisingly, using more advanced DMFT calculations that suggest a very small effective U (< 1 eV). DFT has previously shown that plutonium's 5f electrons are delocalized and analogous to those in uranium metal that are modeled with the same Hubbard U. The latest DMFT modeling results therefore agree with these conclusions.

The contentious matter of magnetism in plutonium has largely been settled since the predicted DFT magnetic form factor and magnetic susceptibility have been validated experimentally. There is no longer any debate—magnetic moments exist in plutonium metal.

Because DFT is fundamentally more transparent and computationally much more efficient than DMFT it makes sense to focus plutonium modeling on this approach. DFT has certainly been very successful in describing many of its anomalous behaviors. Perhaps the greatest achievement of DFT for plutonium has been its ability to reproduce the remarkable ambient-pressure phase diagram with notable accuracy. Some problems, however, have been unresolved for many years. Namely, the bcc (ε) phase is predicted to be mechanically unstable (imaginary phonons) and with an energy that appears quite high relative to the other phases. The ε-Pu instability issue was recently explained by considering anharmonic lattice vibrations from phonon-phonon coupling at finite temperatures. The objective for the present study was to address the remaining question regarding the anomalously high predictions for ε-Pu energy.

Zero-temperature energies for δ and ε plutonium

The large predicted zero-temperature energy for the ε phase, relative to the δ phase for example, may be reasonable if temperature-dependent contributions to the free energy counterbalance it at temperatures where ε-Pu resides.

We investigated this possibility by focusing on the free-energy difference between δ and ε plutonium. In addition to the zero-temperature energy that was obtained from DFT calculations (Fig. 1) we included free-energy contributions

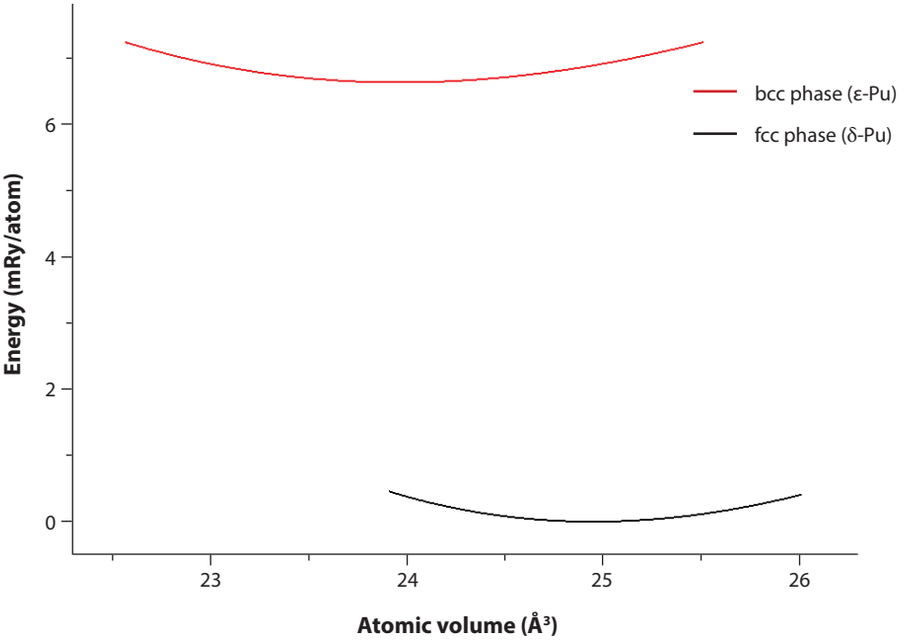

Figure 1. Zero-temperature energies for δ (black) and ε (red) plutonium.

from anharmonic lattice vibrations (F_{vib}), electron-phonon coupling (F_{ep}), magnetic entropy (S_{mag}), and spin fluctuations (F_{sf}). For the anharmonic lattice vibrations, we applied the self-consistent ab initio lattice dynamics (SCAILD) method that includes anharmonicity but not electron-phonon coupling. Because it involves an iterative procedure of demanding calculations of forces on atoms in a supercell, we had to limit our computations to a constant temperature, chosen as 900 K. This lattice-vibration contribution for δ- and ε-Pu was obtained at constant atomic volumes. For δ-Pu it is taken to be the equilibrium volume (the thermal expansion is very small in magnitude) while for ε-Pu the volume was obtained using the Debye-Grüneisen theory with a linear thermal expansion coefficient of 40×10^{-6} K^{-1} that is close to the experimental value (36.5×10^{-6} K^{-1}).

Using the self-consistent ab initio lattice dynamics method

The δ and ε plutonium F_{vib} values as functions of SCAILD iterations are shown in Fig. 2. The converged numbers indicate a difference between ε and δ of 4.0 mRy. The other contributions, F_{ep}, S_{mag}, and F_{sf}, were likewise calculated at 900 K and the thermal-expansion-corrected atomic volumes for the δ and ε phases. In terms of the differences between the phases, F_{ep}, S_{mag}, and F_{sf} contribute 1.4, 0.2, and 1.0 mRy, respectively. Because the zero-temperature energy difference is 6.5 and F_{vib} is 4.0 mRy (Fig. 1) we find that the δ → ε phase transition will occur at 900 K in spite of the large zero-temperature energy difference.

DFT methods

Density-functional theory was applied for two types of calculations. First, the total energies were computed for an anti-ferromagnetic configuration of a face-centered tetragonal phase (AFI) with δ and ε having c/a axial ratios of 1.41 and 1.0, respectively. In the computationally-demanding SCAILD calculations we utilized a 27-atom supercell with an anti-ferromagnetic-type configuration that is similar to AFI. In all these calculations we employed the generalized gradient approximation, spin-orbit coupling, and a small correction due to the f-electron orbital-orbital interaction that is missing in the general formulation of DFT. This orbital polarization correction can be calculated self-consistently and is important for plutonium.

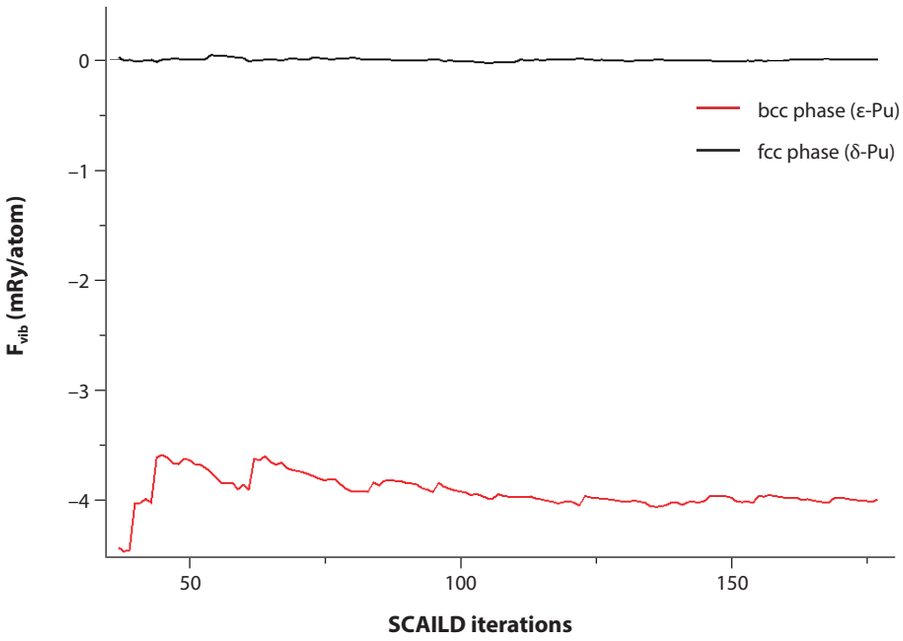

Figure 2. Self-consistent ab initio lattice dynamics (SCAILD) free-energy values (F_{vib}) for δ (black) and ε (red) plutonium as functions of number of iterations.

The full-potential linear muffin-tin orbitals (FPLMTO) method was used for the zero-temperature calculations presented in Fig. 1. Most of the technical details for these calculations are similar to our earlier phase-diagram computations for plutonium. One difference is that the integration over the k points (512 in the irreducible part of the Brillouin zone) is performed using the tetrahedron method for a representation of the electronic structure at zero temperature.

For the computationally-exhausting phonon method we employed the VASP code, which is more efficient than the FPLMTO approach. Because of the importance of both spin-orbit coupling and orbital polarization for plutonium we included these interactions in the VASP-SCAILD calculations (Fig. 2). We recently incorporated a simple variational formulation of orbital polarization in VASP that allows for accurate atomic-force calculations, in conjunction with a correction that correctly accounts for the effect of the $p_{½}$ orbitals on the spin-orbit coupling in Pu. This scheme was employed for the SCAILD free-energy calculations presented in Fig. 2. In this case we broadened the 64 k points with a 900 K Fermi-Dirac distribution function.

Finally, transverse spin fluctuations were modeled in the static limit as disordered spin moments. Therefore we corrected the zero-temperature energies due to the disorder, and as a consequence the ε-δ energy difference decreased relative to the AFI configuration by 1.0 mRy when the spin disorder was accounted for. Longitudinal spin fluctuations are predicted to reduce the spin-moment magnitudes in δ-Pu plutonium but the reduction is similar to ε-Pu and the net effect can therefore be ignored.

Summary

We have calculated the free energy of δ and ε plutonium at constant predicted atomic volumes at 900 K. We found that in spite of having a much higher energy than δ-Pu at zero temperature, the ε phase is favored at high temperatures in agreement with the experimental phase diagram. We found that the most important temperature-dependent contributions to the free energy are the anharmonic lattice vibrations. In this study we have resolved the concern over the high ε-Pu energy in the DFT prediction.

Acknowledgments

We thank A. Landa and L. Yang for helpful discussions. This work was performed under the auspices of the U.S. DOE by Lawrence Livermore National Laboratory (LLNL) under contract DE-AC52-07NA27344 and was partly funded by the Laboratory Directed Research and Development Program at LLNL under Project Tracking Code No. 11-ER-033 and 17-ERD-041.

Cesium Separation from Aqueous Streams Using Calixarene Mono-Crown-Ethers

Marie Simonnet
Japan Atomic Energy Agency (JAEA), Tokai-Mura, Naka-gun, 319-1195 Japan

Cesium-137 is an isotope produced by nuclear fission during the operation of a nuclear power plant. When the Fukushima Daiichi accident occurred in March 2011 following the Tōhoku earthquake, some of the power plant's radioactive material was released, contaminating a large area with ^{137}Cs. This isotope is also particularly troublesome for nuclear waste management—along with ^{90}Sr—because it is the main source of decay heat among the fission products. Coupled with the extraction of minor actinides, removal of Cs from radioactive liquid waste could reduce the cost of safe storage of processed nuclear waste. Studying Cs extraction therefore has a dual application—the cleaning of contaminated water and removal of cesium prior to deep geological repository.

Cesium belongs to the group of alkali elements. Its chemical behavior is therefore similar to sodium (Na) and potassium (K), two relatively earth-abundant elements, and selective separation is challenging. One of the most common separation methods is liquid-liquid extraction, i.e., the transfer of selective particles (ions, molecules) from one liquid to another by mixing; most commonly, one of these phases is aqueous (i.e., the main component is water). In the case of nuclear reprocessing, this phase derives from the previous processing step, dissolution of oxide fuel using nitric acid. It contains a mixture of many different ionic and molecular species, from which a small fraction has to be separated. The other phase meanwhile is organic (i.e., hydrocarbon-based) and contains one or several kinds of organic extractants that are selective towards the desired particles. The extractant is usually diluted by (or, if the extractant is solid, dissolved in) a diluent in order to improve hydrodynamic properties (density, low viscosity) and to lower the quantity of extractant required, which is usually expensive.

Depending on the chemical properties of the extractant, several extraction mechanisms are possible. In this study, neutral species are extracted—cations are therefore extracted along with anions for charge balance. The valence state of Cs in aqueous solutions is +1, therefore one nitrate ion (NO_3^-) is co-extracted for every Cs^+ ion. After the Cs ions are extracted into the organic phase, the two phases are separated. The organic phase is then mixed with another phase (usually aqueous) to recover the extracted elements for further treatment. This latter step is called back-extraction.

In the 1990s, a new class of organic compounds—calixarene crown-ethers—was found to be very efficient for alkali extraction (see Fig. 1). They consist of a "calix" ring (a word derived from the vase-like shape) of four benzene rings, and one (mono-) or two (bis-) crown ether functionalities. In the case of the mono-crown

Marie Simonnet

Marie Simonnet is a Researcher at the Japan Atomic Energy Agency at Tokai-Mura, Japan. She presented her talk titled "Cesium separation from aqueous streams by calix-mono-crown-arenes" *at Pu Futures 2018 in the Nuclear Fuel Cycle II technical session.*

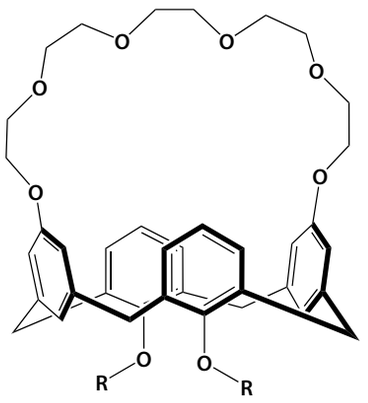

Crown-ether ring
Varied by adding benzene rings *(below)*. Crown-6 (abbreviated **C6**) indicates number of ether groups in crown-ether ring. Rings substituted by one and two benzene rings are termed **BC6** and **DBC6** respectively.

Calix ring
Unchanged in these studies. Number in square brackets **[4]** indicates number of benzene rings.

Dialkoxy chain
Varied by changing the alkyl (R) groups:

octyl	C_8 linear	**DOC**
ethylhexyl	C_8 branched	**DEHC**
dodecyl	C_{12}	**DDC**

Figure 1. The nomenclature and structure of calixarene crown ethers. The calix ring remained unchanged for all studied extractants in this work. Dialkoxy chain length was varied, and benzene linkers were added to the crown-ether ring (*below*). The term *calix* derives from Latin, which translates as "cup" or "chalice", and is used by chemists in this context due to the vase-like shape of the molecule.

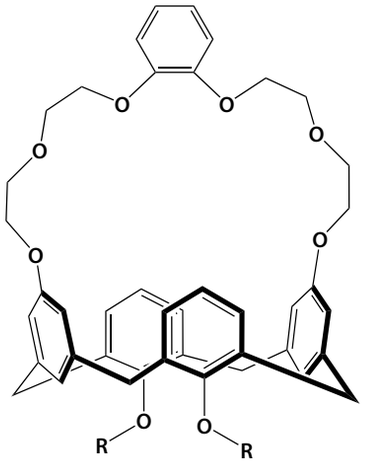

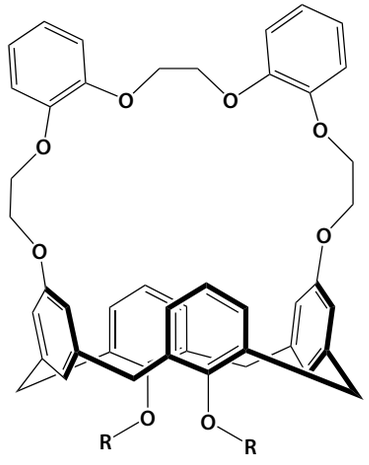

ether, the counterpart is a dialkoxy chain (for example, eight carbons in Fig. 1). Selectivity of the extractant is controlled structurally by the number of ether groups in the crown. For Cs, the highest extraction rate is observed with six O atoms. In that case, very small amounts of Na are extracted, and a high separation can be achieved. The main problem that calixarene crown-ethers present is their very low solubility in most common diluents, requiring the addition of modifiers or the use of specialized diluents.

The aim of this study was to investigate the effects of the main parameters to optimize Cs extraction. The parameters studied were: extractant structure, nitric acid concentration, nitrate salt concentration, and diluent nature.

Extractant structure effect

We studied two types of structural variation: the addition of one or two benzene rings on the crown-ether function, and the variation of the number or the position of carbon atoms in the alkoxy chain. This led to seven different extractants: three di-octyl-oxy (eight linear C atoms on the chain, abbreviation DOC[4]...) with 0, 1, and 2 benzene groups (...[4]C6, ...[4]BC6, and ...[4]DBC6, respectively); three di-dodecyl-oxy groups (12 linear C atoms on the chain, abbreviation DDC[4]...) with 0, 1, and 2 benzene groups and one di-ethyl-hexyl (eight C atoms branched two and six, abbreviation DEHC[4]...) without any benzene groups (Fig. 1, above).

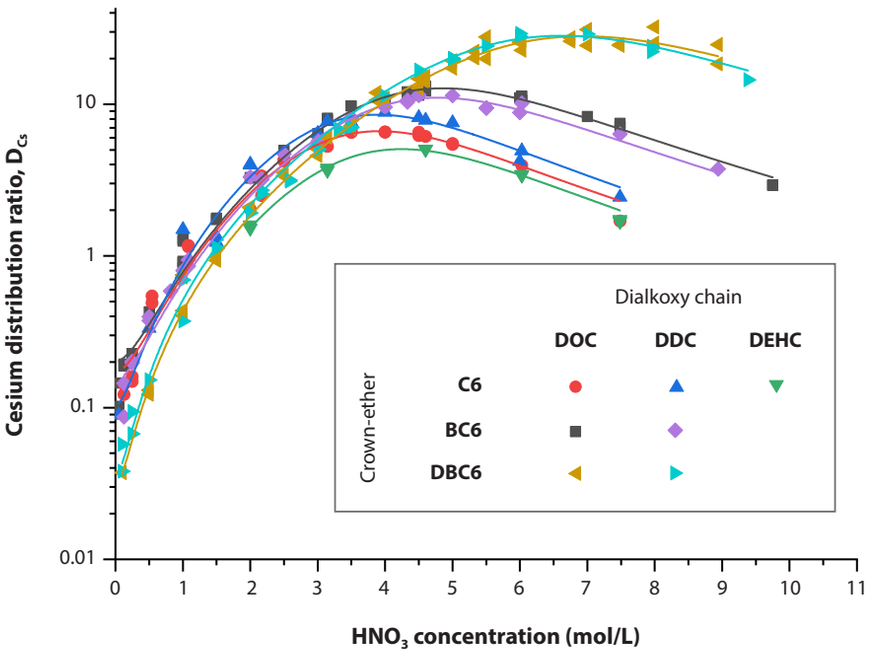

Figure 2. Variation in cesium distribution ratio ($D_{Cs} = [Cs]_{org}/[Cs]_{aq}$, where [Cs] is the concentration of cesium) with the concentration of nitric acid for seven different calixarene crown ethers. Dots are experimental data; lines result from model calculations. D_{Cs} maxima are shifted towards higher nitric acid concentration with the addition of benzene linkers (DBC6, yellow and teal dots, and BC6, black and purple). For these experiments, 0.01 mol/L extractant was dissolved in 2-nonanone.

The Cs distribution ratio, D_{Cs}, defined as the cesium concentration in the organic phase divided by its concentration in the aqueous phase, is plotted versus initial nitric acid concentration in Fig. 2. When greater than 1, cesium has higher content in the organic phase; less than 1, it has higher content in the aqueous phase. We observed that all extractants have a distribution ratio less than 1 at nitric acid concentrations below 1 mol/L, which means that the back-extraction (reverse reaction where the extracted species are recovered in a fresh aqueous solution) is easily achieved in dilute nitric acid or water.

For each system, there is a maximum D_{Cs} value which is due to competitive extraction between Cs^+ and H^+. We can observe that this maximum is shifted towards higher nitric acid concentrations for compounds with an increasing number of benzene rings on the crown-ether ring, meaning that its presence decreases H^+ extraction. Because of the competitive extraction of Cs^+ and H^+, a decrease in H^+ extraction yields higher extraction of Cs^+ ions, so the highest D_{Cs} values are achieved for extractants with two benzene rings. These extractants also show the lowest D_{Cs} values at low nitric acid concentrations, giving the greatest distribution ratio difference between high acidity (extraction condition) and low acidity (back-extraction condition), yielding a better overall efficiency of the whole process.

The separation factors, defined as the ratio of two species distribution ratios, were calculated. As expected, very high Na separation factors were found. It is interesting to note that there is a decrease in Rb and K separation factors with the addition of benzene rings to the crown-ether, however there is an increase for Na. Previously published work states that the addition of benzene rings shrinks the size and increases the rigidity of the crown, resulting in a smaller cavity. The alkali ion size increases with atomic number and therefore the decrease in Rb and K separation factors arises from a better fit in the crown cavity. However, this does not hold true for Na or H_3O^+, most probably because they are extracted along with one or several water molecules, which increases the actual radius of the extracted ion.

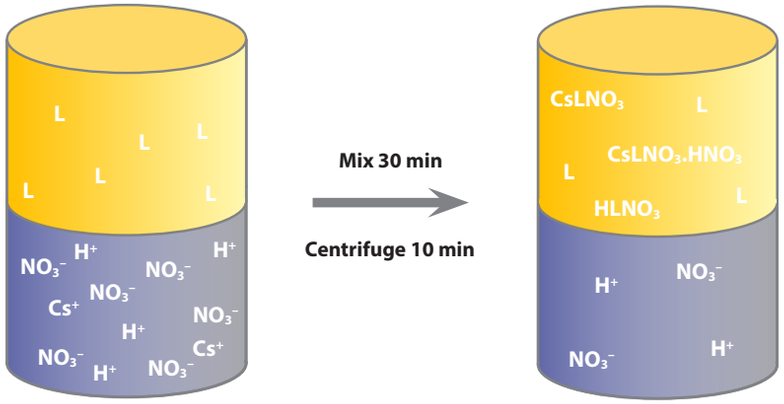

Figure 3. Simplified scheme of extraction process from aqueous phase (blue) into organic phase (yellow) with the assistance of calixarene ligands (L).

Nitric acid effect

To explore the nitric acid effect, we tried to fit the data with several possible models. The best fit, shown as a continuous line in Fig. 2, consists of competitive extraction reactions below (L = calixarene ligand). These reactions are broadly described in an extraction scheme above (Fig. 3). Unexpectedly, it was necessary to consider an additional nitric acid species for the case of ketone diluents. To validate the model, we then studied the nitrate ion effect in isolation.

(1) $Cs^+_{aq} + NO_3^-{}_{aq} + L_{org} \rightleftharpoons CsLNO_3$

(2) $H^+_{aq} + NO_3^-{}_{aq} + L_{org} \rightleftharpoons HLNO_3$

(3) $Cs^+_{aq} + NO_3^-{}_{aq} + H^+_{aq} + NO_3^-{}_{aq} + L_{org} \rightleftharpoons CsLNO_3.HNO_{3\,org}$

(4) $H^+_{aq} + NO_3^-{}_{aq} + H^+_{aq} + NO_3^-{}_{aq} + L_{org} \rightleftharpoons HLNO_3.HNO_{3\,org}$

Nitrate effect

When we replaced nitric acid (HNO_3) with nitrate salts such as sodium ($NaNO_3$) or lithium ($LiNO_3$) in equimolar quantities, a decrease in distribution ratio (D_{Cs}) followed. This was partly due to the different dissociation constants and nitrate activities, which decrease with increasing cation size. However, even at an equal nitrate activity we still observed a difference between $NaNO_3$ and HNO_3, which confirms the mechanism above.

Diluent effect

We compared diluents chloroform (apolar) and 2-nonanone (polar) for performance. D_{Cs} values are much higher for 2-nonanone than for chloroform (Table 1). Consequently, we investigated possible structural differences when changing the diluent. Extended X-ray absorption fine structure (EXAFS) spectroscopy is a very useful tool for atomic-scale studies because this technique allows to determine the average position of the closest atoms surrounding one target element. The principle is to measure the de-excitation energies of the target element electrons after X-ray irradiation. There are small energy oscillations which depend on the number and nature of the neighbor atoms. When calculating the Fourier transform of these oscillations, it is possible to determine the first coordination shells, that is to say the three-dimensional "rings" of atoms that surround the element. In this work, the target element is Cs, and analysis has been performed for two extractants in each diluent.

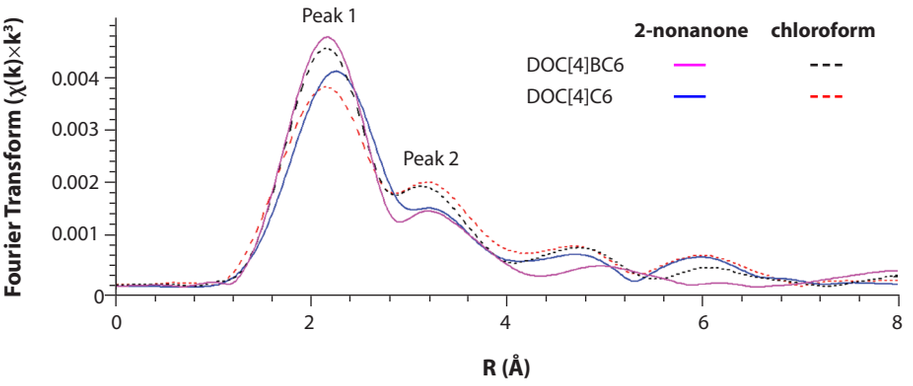

Figure 3. EXAFS spectra of cesium K-edge for two extractants in two diluents. These spectra are representative of the closest atoms surrounding cesium. The first peak, including the neighbor atoms of the first coordination sphere, is seemingly correlated to the extractant nature (BC6 versus C6) while the second peak, representing the neighbor atoms of the secondary coordination sphere, is correlated to the diluent nature (dashed versus solid lines). This change in the secondary coordination sphere with the diluent can explain the distribution ratio differences shown in Table 1. R is the distance before phase correction, measured in angstrom.

Table 1. Comparison of cesium distribution ratios (D_{Cs}) of four extractants in chloroform and in 2-nonanone. Cesium extraction is higher in a polar diluent (2-nonanone) than an apolar diluent (chloroform).

D_{Cs} 3M HNO_3	Chloroform	2-Nonanone
DOC[4]DBC6	3.8	32
DOC[4]BC6	8.6	34
DOC[4]C6	6.4	22
DDC[4]C6	6.5	16

Two main peaks were observed, corresponding to the two closest coordination shells (Fig. 4). When comparing the different systems, variation in the first peak seems to owe an extractant structure change, whereas variation in the second peak is from a diluent nature change. Therefore, both parameters can impact the Cs coordination. A change in coordination environment creates a change in the stability of the complex, which explains why a high difference in D_{Cs} is observed between the two diluents.

Summary

Cesium-137 is a problematic isotope for both nuclear waste reprocessing and accidents such as Fukushima. Its separation is difficult, however, because of the similarities of its chemical behavior to sodium and potassium. It is therefore important to design an efficient process able to separate Cs from other alkali elements. In this work, we studied different parameters that could improve the efficiency of the liquid-liquid extraction process. All the studied parameters, i.e., extractant structure, nitric acid and nitrate salt concentrations, and diluent nature were found to have an impact on cesium extraction, sometimes with correlated effects. Variation of diluent nature showed particularly high differences, including on the local cesium environment and on the extraction mechanism. This observation can be generalized to other extraction systems, in which usually the focus is done on extractant effect only. EXAFS has proven to be a powerful tool to investigate multi-parametric effects at the atomic scale, and more studies could rely on this technique to acquire fundamental knowledge of reaction mechanisms. In the future, it could be valuable to explore the viability of the proposed extraction system on a larger scale, with specific attention to the diluent behavior (using alkylketones).

Freibert to Lead the Seaborg Institute

Franz J. Freibert, Ph.D. has been selected as Leader of the G. T. Seaborg Institute for Transactinium Science at Los Alamos National Laboratory (LANL). As one of six strategic centers within the National Security Education Center, the Seaborg Institute serves to attract, develop, and retain the workforce of actinide scientists and engineers needed to meet the nation's needs, and to integrate research programs on chemical, physical, nuclear, and metallurgical properties of the light actinide elements, with a special emphasis on plutonium, as well as their applications in national security programs.

Freibert brings substantial technical expertise in plutonium materials science, physical properties of plutonium alloys and compounds, thermodynamic properties of phase transformations, and self-irradiation damage and aging effects in plutonium and its alloys. He came to LANL as a Postdoctoral Research Associate in 1996 and afterward joined the technical staff to collaborate on numerous projects and strategic initiatives both at Los Alamos and throughout the Department of Energy National Laboratory Complex. Freibert has been a member of the Seaborg Institute leadership team since 2010. He began as Materials Science Focus Area Leader, contributing to the development and implementation of the Plutonium Science and Research Strategy and in 2014 became Deputy Director. Freibert is internationally recognized as a scientific leader in plutonium materials science, and has served in organizational leadership roles of the Plutonium Futures—The Science international conferences, the International Workshops on the Fundamentals of Plutonium, US/UK JOWOGs, and other technical exchanges.

The broader actinides science and research mission of the Seaborg Institute is directed at maintaining and enhancing U.S. capabilities in actinide science and technology, educating and training Laboratory staff, technicians, students, visiting scientists, and faculty at all educational levels in actinide science, and providing expert advice and forums to address LANL and national issues concerning defense and energy applications of the actinides. The purpose of the Seaborg Institute Education Programs is to provide a broad intellectual community for actinide science and research in support of Laboratory missions and to create a mechanism to attract, retain and pipeline a future generation of actinide scientists and engineers. The Seaborg Institute supports a combination of summer schools, graduate student fellowships, and postdoctoral programs: Seaborg Institute Postdoctoral Fellow Program, Seaborg Institute Summer Research Fellowships, and the Nuclear Forensics Undergraduate Summer School.

" I am extremely optimistic about the future actinides mission at Los Alamos. It is my honor to steward the Seaborg Institute in support of that mission. Success for Los Alamos' 30 pit-per-year mission requires a competent and well-trained workforce who actively engages with confidence, focus, and a healthy sense of scientific curiosity. I am excited about the Seaborg Institute's distinguished role engaging as an institutional partner and leader in the education and development of the current and future Los Alamos scientific and technical workforce "

Franz Freibert, Seaborg Institute Director

Actinide Research Quarterly is published by Los Alamos National Laboratory and is a publication of the Glenn T. Seaborg Institute for Transactinium Science, a part of the National Security Education Center. ARQ (est. 1994) highlights research in actinide science in such areas as process chemistry, metallurgy, surface and separation sciences, atomic and molecular sciences, actinide ceramics and nuclear fuels, characterization, spectroscopy, analysis, and manufacturing technologies.

LA-UR 19-29114

Address correspondence to:
Actinide Research Quarterly
c/o Editor
Mail Stop T-001
Los Alamos National Laboratory
Los Alamos, NM 87545

ARQ can be read online at:
www.lanl.gov/arq

If you have questions, comments, suggestions, or contributions, please contact the ARQ staff at:
arq@lanl.gov

National Security Education Center
David L. Clark, Director

G. T. Seaborg Institute for Transactinium Science
Science Advisors
Franz Freibert, Director
Ping Yang, Deputy Director

Editor
Owen Summerscales

Contributing editors
Susan Ramsay

Designers/Illustrators
Don Montoya
Owen Summerscales
Evan Wells

Photographer
Mick Greenbank

Circulation Manager
Susan Ramsay

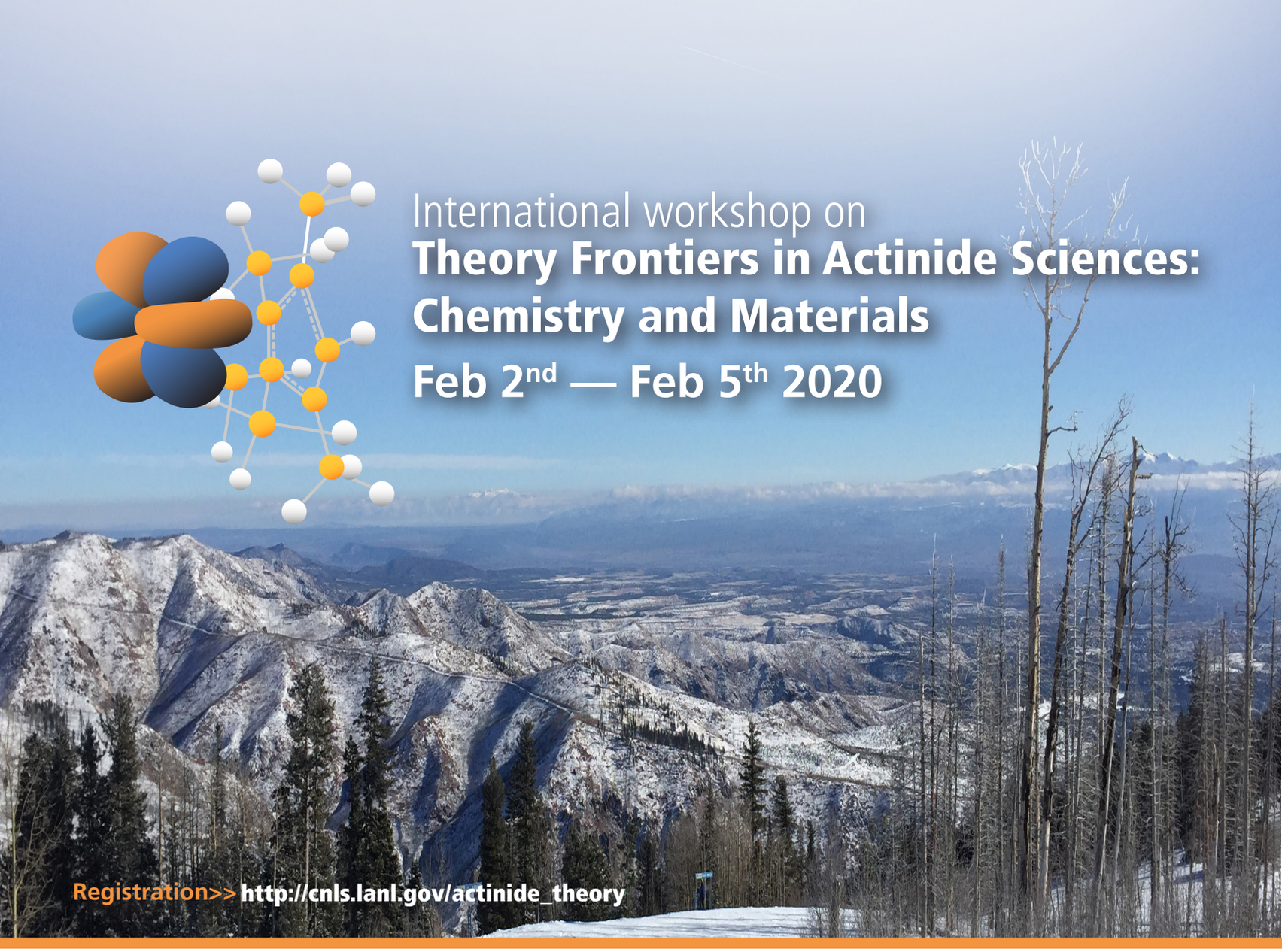

International workshop on

Theory Frontiers in Actinide Sciences: Chemistry and Materials

Feb 2nd — Feb 5th 2020

Registration>> http://cnls.lanl.gov/actinide_theory

Deadline for abstract
Nov 1st 2019

Registration open
Sep 15th 2019

Venue
Hilton at Santa Fe –Santa Fe, NM

Organizing Committee

Ping Yang pyang@lanl.gov
Enrique R Batista erb@lanl.gov
Franz J Freibert freibert@lanl.gov

Sponsors

Seaborg Institute
Center for Non-linear Studies
Los Alamos National Laboratory

Los Alamos NATIONAL LABORATORY EST.1943

NNSA National Nuclear Security Administration